A common molecular logic determines embryonic stem cell self-renewal and reprogramming

Sara-Jane Dunn[1,2,5], Meng Amy Li[2,5], Elena Carbognin[3], Austin Smith[2,4,6*] and Graziano Martello[3*]

[1]Microsoft Research, Cambridge, CB1 2FB, UK

[2]Wellcome Trust - Medical Research Council Cambridge Stem Cell Institute, University of Cambridge, Cambridge, CB2 1QR, UK

[3]Department of Molecular Medicine, University of Padua, Padua, 35131, Italy

[4]Department of Biochemistry, University of Cambridge, Cambridge, CB2 1GA, UK

[5]These authors contributed equally to this work and are listed in alphabetical order

[6]Lead contact

*Correspondence: austin.smith@cscr.cam.ac.uk (A.S.), graziano.martello@unipd.it (G.M.)

Abstract

Reconfiguration of gene regulatory networks is required to instate new cell identities during differentiation and reprogramming. Here we combined automated formal reasoning with experimentation to expose the logic of network resetting for induction of naïve pluripotency. We found that a Boolean network architecture defined for self-renewal accurately predicted reprogramming potency of single or combinations of factors. Deterministic gene activation trajectories were computationally identified and experimentally substantiated at single cell resolution. A counterintuitive observation that Klf2 is required during resetting while dispensable for self-renewal is explained by the contingency of factor availability. We tested 132 predictions formulated by the dynamic network, finding a predictive accuracy of 79.6%, and further show that this network accurately explains experimental observations of somatic cell reprogramming. We conclude that a common and deterministic program of gene regulation governs both self-renewal and induction of pluripotency. The methodology could be applied to delineate dynamic networks underlying other cell fate transitions.

Introduction

Over the last 10 years a multitude of protocols have been developed that allow the conversion of one cell type into another[1]. Most of these strategies rely on the forced expression of transcription factors (TFs) highly expressed by the target cell type that have either been chosen empirically or, recently, with the aid of computational tools such as CellNet or Mogrify[2–4]. Despite the large amount of transcriptomic data available for such conversions,

our understanding of the dynamics and logic followed by cells during reprogramming and transdifferentiation remains fragmentary.

The most studied cell fate transition is the generation of murine induced pluripotent stem cells (iPSCs) from somatic cells[5]. Bona fide iPSCs are, like murine embryonic stem cells (ESCs), competent to form blastocyst chimaeras, and are considered to occupy a state of naïve pluripotency similar to that in the pre-implantation embryo[6,7]. This unique identity is determined by a self-reinforcing interaction network of TFs. Experimental and computational efforts have led to circuitry mapping of the core TF program that maintains ESC self-renewal under defined conditions[8–14].

We previously applied a mathematical and computational modelling approach based on automated formal reasoning to elucidate the regulatory network architecture for self-renewing mouse ESCs[9,15]. A minimal interaction network of 12 components was found to recapitulate a large number of observations about ESC maintenance, and successfully predict non-intuitive responses to compound genetic perturbations[9].

Forced expression of several components of this core TF network in various cell types leads to a state of induced pluripotency[5,16–25]. Accumulating evidence suggests that cells progress through defined stages, with a final transition entailing the hierarchical activation and stabilisation of the naïve pluripotency TF network[16,17,26–33]. This suggests that maintenance and induction of naïve pluripotency could be under the control of the same TF network

architecture. However, it is not clear if cells undergoing conversion follow a deterministic trajectory of gene activation, defined by the naïve pluripotency TF network architecture, or if genes are activated in random sequence.

A tractable experimental system with which to investigate activation of the naïve pluripotency network is the resetting of post-implantation epiblast stem cells (EpiSCs)[34]. EpiSCs are related to gastrulation stage epiblast[35,36]. They represent a primed state of pluripotency, developmentally downstream of the naïve state[6] and unable to contribute substantially to blastocyst chimaeras. EpiSCs exhibit distinct growth factor, transcriptional and epigenetic regulation compared to ESCs. They self-renew when cultured in defined media containing FGF2 + ActivinA (F/A)[34,37,38]. These cells invariably lack significant expression of functionally defined naïve pluripotency factors, with the exception of Nanog. EpiSC resetting proceeds much faster than somatic reprogramming over 6-8 days and entails primarily the activation and consolidation of naïve identity[39–42]. In addition, EpiSC resetting does not require a complex reprogramming cocktail. The activation of Jak/Stat3 signalling[21,43,44] or forced expression of a single naïve TF factor[21,33,34] is sufficient to mediate reprogramming in combination with dual inhibition (2i) of the Erk pathway and glycogen synthase kinase-3 (GSK3)[45].

In this study, we undertook an iterative computational and experimental approach to test the hypothesis that a common network governs both naïve state maintenance and induction. Focusing on EpiSC resetting, we investigated whether naïve state induction follows an ordered sequence of network component activation. By refining our understanding of the

network governing this process, we sought to uncover genes crucial for the execution of resetting, to accelerate resetting dynamics, and thereby to enhance the overall efficiency. Finally, we investigated whether the same network architecture is also utilised in somatic cell reprogramming.

Results

Deriving a Set of Models Consistent with EpiSC Resetting

We previously studied the TF network controlling maintenance of naïve pluripotency[9] through a combined computational and experimental approach. Our methodology is based on the definition of relevant network components, delineated from functional studies in the literature, and the identification of 'possible' interactions between these components (Fig. 1a). Possible interactions are inferred based on gene expression correlation using the Pearson coefficient as a metric (Methods), and are used to define a set of concrete Boolean network models, each with unique topology. We refer to this as an Abstract Boolean Network (ABN). We then define a set of experimental results, such as the effects of genetic perturbations, that serve as constraints to identify those models from the ABN that are relevant to the biological process of interest. The Reasoning Engine for Interaction Networks (RE:IN, www.research.microsoft.com/rein) is software developed to synthesise only those concrete models that are consistent with the experimental constraints[9,15]. A set of consistent models is thereby derived, which we define as a constrained Abstract Boolean Network (cABN). This approach differs from typical modelling strategies in the fact that we do not generate a single model, but rather a set of models that are consistent with known behaviours. We formulate predictions of untested behaviour only when all models agree, such that predictions are

consistent with the limits of the current understanding of the network. This is important as often different network models can recapitulate experimental observations, and one cannot prioritise one model over another. The predictions are then tested experimentally. Whenever predictions are falsified by experimental results, it is possible to refine the set of models by incorporating the novel findings as additional constraints (Fig. 1a). The refined cABN is then used to generate further predictions.

For the present study, we first refined the cABN describing maintenance of naïve pluripotency, defined by a Pearson coefficient threshold of 0.832 (Fig. 1b, S1a-c), by adding further expression profiles generated using RNA-sequencing and RT-qPCR to the five datasets used previously[9] and by using an updated version of RE:IN[15] (Methods). We tested the refined naïve state maintenance cABN (Fig. S1d) against novel gene perturbation experiments in mouse ESCs and observed a significant increase in prediction accuracy over the previous version and therefore used this for further analyses.

We next asked whether the maintenance cABN is consistent with experimental observations of EpiSC resetting. To this end, we exploited GOF18 EpiSCs, which are susceptible to resetting in 2i+LIF in the absence of transgenes[21]. In accordance with the Boolean modelling formalism we use, we discretised gene expression patterns of our network components for the initial (GOF18 EpiSC) and end point (naïve state ESC) cell types, such that each gene is High/Low in each case (Fig. S1e and Methods). We defined a set of six reprogramming constraints based on known conditions under which EpiSC resetting can or cannot be achieved (Fig. 1c, Fig. S1e Methods). For example, one constraint specifies that if a given cell has none of the pluripotency factors initially expressed, then 2i+LIF alone is insufficient to induce the naïve

state (Fig. 1c, top arrow). In contrast, resetting can be achieved if we instead start from GOF18 EpiSCs, which already express Oct4, Sox2 and Sall4 (third arrow down from the top). We found that these additional constraints were satisfied by the set of models that already satisfied the maintenance constraints, suggesting that a single cABN controls both maintenance and induction of naïve pluripotency.

The number of concrete models in the 0.832 cABN is on the order 10^5. As a control, we randomly generated 10,000 models with the same number of components and possible interactions as the 0.832 cABN. None of these models could satisfy the entire set of constraints. The probability of generating a model consistent with the experimental observations by random interaction selection is of the order 10^{-49}. Therefore, the data-driven approach facilitated identification of meaningful interactions between network components, and in practical terms substantially reduced the compute time for subsequent analyses.

The dynamics of the concrete networks in the cABN were determined by a synchronous update scheme: from a given initial condition, each and every component updates its state in response to its upstream regulators at each step. Accordingly, we could examine the sequence of activation of each component along the trajectory towards the naïve state. Fig. 1d shows the ordered activation of naïve network components during conversion of EpiSCs to naïve iPSCs upon 2i+LIF induction over 5 regulation steps in one concrete network from the 0.832 cABN. RE:IN can determine the number of regulation steps required for all models to reach the naïve state. This can be used as a metric to study the resetting process (Methods).

Prediction of Resetting Potency for Individual Network Components

It has been reported that spontaneous EpiSC resetting can be enhanced by expression of naïve network factors, such as Klf2[40,41,46], and that such resetting events, measured by reporter activation, often possess faster activation kinetics than control[40]. In our case, the GOF18 EpiSC line contains a transgenic GFP reporter driven by the upstream regulatory region of Pou5f1 (Oct4). The transgene does not behave as endogenous Oct4, which is uniformly active in EpiSCs and ESCs, but serendipitously allows the live monitoring of resetting events[21]. We hypothesised that enhanced resetting efficiency is due to accelerated activation of the naïve network. We sought to test this computationally by determining the number of regulation steps required for *all* concrete models of the cABN to stabilise in the naïve state in 2i+LIF, with or without Klf2 transgene expression. Analysis of the set of models predicted that forced expression of Klf2 in GOF18 EpiSCs results in the network stabilising in the naïve state in only 3 steps, compared with 5 steps for parental GOF18 (Fig. S2a). Experimentally, we confirmed that transient Klf2 expression induced Oct4-GFP+ iPSC colony formation earlier than empty vector control and led to higher colony number at the endpoint (Fig. S2b, day 6 vs day 10)[40]. Thereafter, we assumed that the number of Oct4-GFP^{+} colonies obtained reflected resetting dynamics and used this as an experimental output to compare with computational predictions.

We analysed the effect of forced expression of each network component using the 0.832 cABN (Fig. 1e). The predictions indicated that expression of certain factors would lead to stabilisation in the naïve state in fewer steps than control, indicating that such factors could play an enhancing role, leading to faster resetting kinetics. For example, when Esrrb is

introduced, all concrete models predicted full activation of the naïve network by step 2, compared to 5 steps for control.

To test these predictions experimentally, we cloned individual network components into an identical vector backbone, and transiently transfected GOF18 EpiSCs with each factor one day prior to resetting initiation in 2i+LIF. We measured the relative efficiency between different components by the fold increase of Oct4:GFP^{+} colonies formed at day 7 over empty vector control (Fig. 1f). While some factors, such as Sall4 and Oct4, had no significant effect over control, others, notably Esrrb, Klf2, and Klf4, showed a robust enhancement. The computational predictions showed a similar general trend to the experimental results, with seven out of eleven cases correctly predicted. Predictions for Tbx3, Stat3 and Oct4 transgene expression were incorrect, however. Most strikingly, Sall4 was predicted to be one of the most efficient factors, but was found to be the least efficient experimentally.

The iterative nature of our approach allows us to refine the set of models in the light of new experimental results that were incorrectly predicted. We encoded the experimental observation that Sall4 expression was no more efficient than control as an additional constraint (Methods). To satisfy the new constraint together with the original set, we increased the number of possible interactions by lowering the Pearson coefficient threshold to 0.782 (Fig. 1g). This new threshold was not chosen arbitrarily, but rather was the highest threshold to define a set of models that satisfy the updated experimental constraints. We subsequently generated a new set of predictions for all single factor forced expressions (Fig. 1h). In each case, we observed a range of steps for which some concrete models predict

stabilisation in the naïve state, while others do not (Fig. 1h, light green). Given that the cABN implicitly defines a set of models that are consistent with all the imposed experimental constraints, each concrete model must be considered equally valid. Therefore, predictions can only be formulated when all concrete models are in agreement (Fig. 1h, dark green). This resulted in predictions that Esrrb, Klf4, Gbx2, Klf2 and Tfcp2l1 single expression are more efficient than control, in agreement with the experimental results in Fig. 1f.

For forced expression of Nanog, Tbx3, Stat3, and Sox2, overlap of the light green regions with control prevented definitive predictions. To resolve this uncertainty, we formally tested *in silico* whether for every concrete model expressing a given gene would be more efficient than control. This resulted in the correct predictions that Nanog was always at least, or more efficient than control, while Stat3, Sox2 and Oct4 were not. This strategy did not generate a prediction for Tbx3 because different models display different kinetics (Fig. 1h, light green region). Note that the lack of effect of forced expression of Sall4 has been imposed as a constraint, and is no longer considered to be a prediction.

We extended the test to perform a pairwise comparison of all gene pairs so as to delineate the relative efficiency between factors (Fig. S2c). Predictions could be formulated for 42 out of 66 possible pairs. Of these, 26 were supported experimentally, while 10 were incorrect. For the remaining 6, the experimental results showed a trend in agreement with the predictions, although without reaching statistical significance due to variability in the naïve colony number between independent experiments. Fig. S2d summarises all significant pairwise comparisons with experimental support.

Delineating the Sequence of Network Activation

The cABN accurately predicted the effect of forced expression of naïve components on resetting efficiency, which suggests that resetting is not a random process. We therefore asked if resetting occurs via a precise sequence of gene activation, and whether this could also be identified using the cABN. Fig. 1d illustrates how one example concrete model stabilises in the naïve state through a sequence of gene activation. We investigated whether a defined sequence of gene activation was common to all concrete models, or whether individual models transition through unique trajectories. We focussed on those genes expressed at low levels in GOF18 EpiSCs, to enable unequivocal detection of activation over time in population-based measurements.

To predict the sequence of gene activation during resetting, we examined the number of regulation steps required for each gene to be permanently activated in 2i+LIF without transgene expression (Fig. 2a). For Stat3, Tfcp2l1, Gbx2 and Esrrb, all models were in agreement, predicting that Stat3 and Tfcp2l1 are activated early, while Gbx2 and Esrrb are activated late. Klf2 and Klf4 were predicted to be activated between these early and late sets, while the range of step values for permanent Tbx3 activation predicted by models within the cABN prevented a definitive prediction. Based on these seven genes, all models follow a similar sequence of gene activation during the initial and final steps of resetting, with an intermediate phase where variations in Tbx3, Klf2 and Klf4 expression are compatible with multiple possible trajectories.

To test these predictions, we measured the expression of each gene over the 2i+LIF resetting time course for up to 4 days (Fig. 2b, c). We defined gene activation to be an induced

expression level that is statistically significant over EpiSCs in F/A. As predicted, Stat3 was significantly induced over its initial GOF18 level as early as 2 hours after 2i+LIF induction, Tfcp2l1 after 8 hours, while Klf4 and Esrrb only became detectable at 48 hours. In contrast to the predictions, Klf2 was significantly induced after only 1 hour of 2i+LIF treatment. Taken together, the population based gene expression profiling indicated that Stat3, Tfcp2l1 and Klf2 were early-activated factors, while Klf4, Tbx3 and Esrrb were late-activated factors.

Tfcp2l1 and Esrrb are direct targets of the LIF/Stat3 and CH/Tcf3 axes[42,46–48]. However, even though CH and LIF were applied simultaneously to initiate resetting, Tfcp2l1 and Esrrb displayed very distinct activation kinetics. We hypothesised that the local regulation topology of these two components may affect the timing of their activation. We therefore examined all immediate upstream regulators of Tfcp2l1 and Esrrb, and the logical update rules that define when each component would become active (Fig. 2d). Tfcp2l1 has six upstream activators, of which Stat3 and Esrrb are definite, and one inhibitor, Tcf3. Esrrb has three definite activators, Sall4, Nanog and Tfcp2l1, as well as a definite and an optional inhibitor. The computational methodology defines a set of 9 alternative update rules, referred to as regulation conditions, that span all the possible scenarios under which a target can be activated. In the same manner in which some possible interactions were found to be required or disallowed when experimental constraints were applied to the ABN, certain regulations conditions were also found to be used or unused across the cABN in order to satisfy the constraints. We compared the subset of regulation conditions assigned to Tfcp2l1 and Esrrb across all models, and one key difference emerged. While Tfcp2l1 required only one of its potential activators (Stat3, Esrrb, Tbx3, Gbx2, Klf2 or Klf4) to activate expression, Esrrb required the presence of all its activators (Nanog, Tfcp2l1, Sall4) (Fig. 2d). Since Stat3 was

activated very early in response to 2i+LIF, early activation of Tfcp2l1 could therefore be attributed to Stat3 activity. Esrrb would only be activated after activation of Tfcp2l1. This local topology analysis therefore provides a network explanation accounting for the early activation of Tfcp2l1 and late activation of Esrrb.

Combinations of Factors Can Enhance Resetting Efficiency

Earlier studies have shown that forced expression of a combination of factors can synergistically enhance resetting efficiency[40,44,46]. Our computational approach enabled us to investigate the effect of factor combinations in a systematic manner. We focused on those factors found to be potent inducers when expressed individually: Klf4, Klf2, Esrrb, Tbx3 and Tfcp2l1 (Fig. 1f). Six out of seven pairwise combinations were predicted to reduce the number of regulation steps required to induce and stabilise the naïve state (Fig. 3a, left). In the case of Esrrb/Tfcp2l1 dual expression, no enhancement beyond single factors was predicted.

We transiently transfected EpiSCs with dual factors to test these combinations experimentally. The number of reset GFP^+ colonies was scored at day 7 and resetting efficiency was calculated based on fold increase over empty vector control. Six out of seven experimental results were consistent with computational predictions (Fig. 3a, right). Five combinations (Esrrb/Klf2, Esrrb/Klf4, Esrrb/Tbx3, Klf4/Tbx3, Klf2/Tbx3) yielded synergistic enhancement, while two combinations (Esrrb/Tfcp2l1 and Klf2/Klf4) demonstrated no greater effect than the single factors (Fig. 3b). These results show that the modelling approach reliably predicts which dual factor expression can render the resetting process more efficient, and the network topology can explain why certain pairs combine synergistically to accelerate

the process (Fig. S3). This demonstrates that taking only network topology into consideration is largely sufficient to predict synergistic and non-additive behaviour of factor combinations.

Since dual expression of Esrrb/Tbx3 and Esrrb/Klf4 dramatically enhanced resetting, we utilised these combinations to explore resetting dynamics in detail. To this end, we generated *PiggyBac* vectors harbouring doxycycline (DOX) inducible Esrrb-T2A-Klf4-IRES-Venus and Esrrb-T2A-Tbx3-IRES-Venus constructs. We delivered the transgenes into GOF18 EpiSCs together with a separate rtTA construct (Fig. 3c). The presence of Venus$^+$ cells upon DOX treatment confirmed induction of transgene expression. As a control, we used an empty vector carrying only the DOX responsive element and IRES-Venus. To assay resetting potency, we transferred EpiSCs to 2i+LIF in the absence or presence of DOX (0.2 µg/ml) for 48h, and continued resetting in 2i+LIF only for an additional 4 days before scoring Oct4-GFP$^+$ colonies (Fig. 3d, e). Cells transfected with the empty vector with or without DOX, or with expression constructs in the absence of DOX, showed spontaneous resetting at low frequency, as expected. In contrast, both factor combinations in response to DOX yielded robust Oct4-GFP activation. There were too many GFP$^+$ colonies to score accurately, therefore we quantified the GFP signal intensity of randomly selected fields (Fig. 3e, bottom panel). This analysis demonstrated that DOX induction led to a 9-16 fold increase in the total Oct4-GFP.

To examine resetting kinetics functionally, we replated cells after 2, 4, 6, or 8 days (Fig. 3d) at clonal density and scored the number of Alkaline Phosphatase (AP) positive colonies that formed. In the absence of DOX, both the empty vector and dual expression transfectants exhibited gradual accumulation of a few colonies. After induction with DOX, however, dual

factor transfectants displayed rapid production of numerous AP^+ colonies, commencing as early as day 2 and peaking at day 6 (Fig. 3f).

To investigate whether the effect of these two factor combinations extended to other EpiSC resetting systems, we expressed these combinations in an independent EpiSC line, OEC2, which carries an Oct4-GFP transgene and the chimeric LIF receptor GY118[44]. Resetting does not occur in this cell line in 2i+LIF alone. Similar to GOF18 EpiSCs, we found robust induction of Oct4-GFP^+ colony formation with DOX treatment, and could observe resetting to the naïve state with only 24 hours of DOX induction (Fig. S4a-e).

Delineating the Sequence of Network Activation upon Dual Factor Expression at Single Cell Resolution

We next used the cABN to investigate the sequence of gene activation that occurs upon dual factor expression. Predictions were generated for the number of regulation steps required for each component to be permanently activated (Fig. 4a, b top, Fig. S3), and compared with experimental results (Fig. 4a, b bottom). To generate the experimental results, we measured network component expression of DOX-inducible GOF18 EpiSCs carrying the empty vector, Esrrb-T2A-Tbx3 or Esrrb-T2A-Klf4 constructs, and treated with 2i+LIF in the presence or absence of DOX.

Under DOX treatment, Esrrb-T2A-Tbx3 transfectants showed a more robust activation of endogenous Klf2 and Klf4 in the presence of DOX at day 4 relative to non-induced cells, consistent with the prediction that these genes should be activated earlier than empty vector

control. Stat3 upregulation was not accelerated, as predicted. However, in the case of Tfcp2l1, we detected enhanced activation that was not predicted. For Esrrb-T2A-Klf4 expression, we observed accelerated activation of Klf2 and Tbx3 at day 4 compared to control, consistent with predictions. Again, we observed enhanced activation of Tfcp2l1 that was not predicted, while Stat3 showed no enhancement over control. Importantly, the sequence of gene activation was consistent with OEC2 EpiSCs (Fig. S4f).

To delineate the sequence of events in resetting progression, we investigated Esrrb-T2A-Klf4 driven resetting at single cell resolution. We sorted individual cells after 2 and 4 days in 2i+LIF with DOX treatment. We conducted single cell gene expression profiling by RT-qPCR of those cells that were productive in resetting, i.e. Day 2 Venus/GFP Low and High and Day 4 Venus/GFP High cells that were clonogenic (Fig. 4c). As controls, we included mouse ESCs (RGd2)[49] and un-induced parental EpiSCs. We profiled selected genes that are differentially expressed between naïve ESCs and primed EpiSCs along with core pluripotency factors Oct4 and Sox2 (Fig. 4 d, e, Table S1). Robust activation of naïve state associated genes was observed in Day 4 Venus/GFP High cells. Some genes, such as Oct4 and Nr5a2, showed even higher expression than in ESCs (Fig. 4d), possibly due to perduring expression of Esrrb and Klf4. Oct4 and Sox2 were reduced in many, but not all, Day 2 Low cells, but were robustly expressed in some Day 2 High and all Day 4 High samples. EpiSC enriched genes that are also expressed at low levels in naïve ESCs, such as Otx2, Utf1 and Pim2, were downregulated at day 2. However, some Day 4 High cells re-acquired expression of those genes which are associated with early transition from naïve pluripotency[49,50]. Overall, the single cell transcriptional analysis further validated the robust, stable activation of the naïve network after 4 days of Esrrb-T2A-Klf4 expression. We assayed the naive network and transitional markers in established reset

clones at passage 3, and found that their expression levels were similar to those in established ESCs (Fig. S5a). Finally, contribution to live-born chimaeras after blastocyst injection of two reset clones confirmed naïve pluripotent identity after resetting by Esrrb/Klf4 dual expression (Fig. S5b).

Clustering of Single Cell Gene Expression Profile Reveals a Resetting Trajectory

We explored the sequence of gene activation at single cell resolution by examining the proportion of cells displaying expression of individual genes at different stages of resetting to test whether these data were consistent with predictions. For example, the cABN predicted that Klf2 would always be active before Tbx3, from which it follows that upregulation of Tbx3 should not occur in the absence of Klf2.

We discretised the data by k-means clustering (Methods), in order to calculate the proportion of cells at each resetting stage exhibiting each of four expression patterns: Klf2/Tbx3 both Low; Klf2 High and Tbx3 Low; Klf2/Tbx3 both High; and Klf2 Low and Tbx3 High (Fig. 5a, top row). The majority of cells at Day 2 were Klf2/Tbx3 double negative, while such cells were not found at Day 4, nor in ESCs. By Day 4, the majority of cells were Klf2/Tbx3 double positive as for ESCs. We observed subpopulations in which Klf2 was High and Tbx3 was Low, mostly at Day 2 with Day 2 High cells containing more than Day 2 Low cells, while a negligible fraction of cells was Tbx3 High, Klf2 Low. This is consistent with the prediction that Klf2 precedes Tbx3 activation during resetting upon Esrrb-T2A-Klf4 expression. Even when all cells were considered together, irrespective of resetting stage, only rare cells exist in the Klf2 Low and Tbx3 High expression state. Importantly, a similar fraction of such cells was found in the ESC

population, indicating that they most likely reflect transcriptional fluctuation or heterogeneity in the naïve state. Similarly, the cABN accurately predicted that Klf2 will be high before Gbx2 activation, and sustained expression of Sox2 precedes Tfcp2l1 activation (Fig. 5a, middle and bottom panels).

To visualise the potential cellular hierarchy during resetting progression, we analysed the single cell profiles using the SPADE algorithm[51,52]. Hierarchical clustering implemented by SPADE successfully grouped the five different populations that we profiled. Based on pluripotency marker expression, we furthermore defined three branches of cells with consistent transcriptional profiles and functional properties. Parental EpiSCs and Day 2 Low cells were positioned in one branch of the SPADE tree (Fig. 5b, black line). Such cells cannot form reset naïve cells upon re-plating (Fig. 4c) and displayed low expression of all pluripotency markers. A second SPADE branch comprised Day 2 High cells, and a minority of Day 2 Low cells, where the core factors Oct4 and Sox2 were expressed, together with early naïve factors such as Klf2 and Tfcp2l1 (blue line). Finally, Day 4 High cells and ESCs, which displayed comparable capacity to form colonies (Fig. 4c), clustered together in one SPADE branch, characterised by high expression of core, early and late naïve pluripotency markers (green line). This analysis also allowed us to place factors that are not in the naïve network on to the resetting activation timescale. For example, Nr5a2, a known resetting enhancing factor[53], activates in a similar pattern to Klf2 throughout resetting.

Identifying Required Components for Naïve Network Activation

We then investigated whether loss of specific network factors would either delay or block naïve network activation. By formulating test hypotheses in a similar manner to single factor expression analyses, we used the cABN to predict the required network components by investigating whether the network could permanently reach the naïve state in the absence of each factor (Fig. 6a). The 0.782 cABN predicted that two factors, Esrrb and Gbx2, are dispensable for resetting, while the remaining factors are required. In the case of Tbx3 no prediction could be formulated.

To test these predictions, we transfected siRNAs against individual network factors into GOF18 EpiSCs, and initiated resetting 24 hours post transfection by switching from F/A to 2i+LIF. We scored the number of Oct4-GFP^{+} colonies at day 6, and calculated the percentage clonogenicity relative to control siRNA transfected cells (Fig. 6b). Experimental results confirmed that Gbx2 is dispensable for resetting, and revealed that loss of Gbx2 actually enhanced resetting efficiency. Furthermore, the requirement for Oct4, Sox2, Stat3, and Klf2 were accurately predicted. Knockdowns of Esrrb and Tbx3 reduced but did not abolish colony formation. Overall, 5 out of 7 predictions were consistent with experimental results.

The experimental results revealed distinct resetting behaviour upon Klf2 or Klf4 depletion. Both were predicted to be required, yet Klf4 knockdown did not eliminate colony formation, while Klf2 was found to be essential. This experimental result was counterintuitive as well as not predicted. Klf4 and Klf2 show at least partially redundant function in ESC self-renewal[54],

and both were potent resetting inducers when expressed in GOF18 EpiSCs (Fig. 1f). To confirm the result, we generated Klf2 and Klf4 knockout (KO) GOF18 EpiSCs by deleting the largest coding exons using CRISPR/Cas9 (Fig. S6a, b). Resetting in 2i+LIF using two independent KO EpiSC clones confirmed the knockdown results: Klf4 KO EpiSCs generated Oct4-GFP$^+$ colonies as efficiently as control cells, while Klf2 KO EpiSCs yielded no Oct-GFP$^+$ colonies (Fig. 6c). This observation was further validated using an independent EpiSC line in which resetting is driven by hyperactivation of Stat3 (Fig. S6d).

To investigate the specific consequence of Klf2 loss for network activation, we examined the expression of network components in WT and Klf2 KO cells over the resetting time course for up to 4 days (Fig. 6d). WT and KO cells showed similar patterns of expression for Oct4, Sox2 and Sall4. For up to 8 hours of resetting, Klf2 KO cells behaved similarly to WT. However, Klf2 KO cells failed to elevate the expression of Nanog and Tfcp2l1 at later time points. Those factors initiated late during resetting in control cells - Esrrb, Klf4, and Tbx3 - failed to be activated in Klf2 KO cells. Taken together, these data suggest that in the absence of Klf2, early factors can initially respond to 2i+LIF, but this response is not sustained, and the activation of late factors fails. Of note, EpiSC markers - Pou3f1, Otx2, Fgf5 - were sharply downregulated in both WT and KO cells, suggesting that Klf2 is not involved in the dissolution of EpiSC identity. Furthermore, in both WT and Klf2 KO EpiSC resetting we observed upregulation of lineage-specific genes, such as Sox1 and Pax6 (ectoderm), T/Bra (primitive streak), Flk1 (mesoderm) and Pdgfrα (endoderm) at the population level. In the absence of Klf2, we did not detect increased expression of any particular markers, suggesting that it does not exert a lineage repression function during resetting.

We asked whether forced expression of individual network factors could compensate for the loss of Klf2. To this end, we transiently expressed all individual factors and found that only Klf2 and Klf4 could rescue the Klf2 KO phenotype (Fig. 6e). These results indicate that Klf2 is specifically required for initiating resetting in EpiSCs. Rescue by forced expression of Klf4 suggests that the two factors are functionally equivalent and that differences in the activation kinetics of the two factors during resetting (Fig. 2b) underlie the requirement for Klf2 and dispensability of Klf4 (see also Discussion).

We picked and expanded individual Klf2 KO reset clones obtained via transient Klf2 expression at day 7, and confirmed they were free of integration of Klf2 transgene by genomic PCR (Fig. S6c) and lack of Klf2 expression (Fig. S6e). We quantified gene expression for naïve network factors in these lines, and found that Oct4, Tbx3, Tfcp2l1 and Klf4 levels were comparable to control, while Sall4, Gbx2, Sox2, Stat3 and Nanog were elevated (Fig. S6e). Only in the case of Esrrb was gene expression lower in Klf2 KO iPSCs than in control. Despite these differences, Klf2 KO naïve cells showed sustained self-renewal. Therefore Klf2 is dispensable for maintenance in 2i+LIF once naïve pluripotency has been attained, consistent with previous reports for ESC propagation[55].

The differential requirement for the two Klf factors was not recapitulated by our modelling. Therefore, we added an additional constraint to specify that Klf4 is dispensable for resetting. To satisfy this constraint by allowing additional possible interactions, the Pearson coefficient was lowered to 0.76. The resulting 0.76 cABN was fully consistent with siRNA knockdown phenotypes in resetting (Fig. 6f left, compared to 6a).

In light of the unexpected finding that Klf2 was specifically required for resetting, we investigated the relevance of other network components for resetting versus maintenance of naïve pluripotency. Predictions were generated and tested by siRNA transfection in self-renewing ESCs followed by clonal assay[9]. Stat3 and Klf2 emerged as factors specifically essential to resetting, while other factors are either dispensable for both (Klf4 and Gbx2) or essential to both (Oct4 and Sox2) (Fig. 6f). These results indicate that resetting and maintenance display different requirements for network components, and that such differences are correctly identified by the cABN.

A Single Biological Program Governs Maintenance and Induction of Naïve Pluripotency

The 0.76 cABN was used to reformulate predictions for all experimental observations generated for both naïve state maintenance[9] and EpiSC resetting (Table S2). In total, the 0.76 cABN is constrained against 44 experimentally-observed behaviours, and generated a further 132 predictions that are consistent with experimental results (Supp. Material). For comparison, we reference the cABN described by Dunn et al.[9], as well as the 0.782 cABN (Fig. 6h, Table S3). Importantly, we observed a progressive improvement as we refined the set of models against new experimental data: the number of predictions that could be made increased from 79 to 283, and the predictive accuracy both for naïve state maintenance and resetting reached 79.6%. Interestingly, this rich set of behaviours can be explained by only 29 interactions between all network components in two alternative “minimal” network topologies (Fig. 6i). We characterised both required and disallowed interactions in the 0.76 cABN against CHIP-sequencing data generated from self-renewing mouse ESCs[56] and found that 72.2% are supported (Table S4). This suggests that a large fraction of the interactions may be direct.

To test the explanatory power of the 0.76 cABN in the context of naïve network installation from somatic cells, we first surveyed the literature for those combinations of factors present in our network that have been used to reprogram mouse embryonic fibroblasts (MEFs). Without encoding any additional constraints, the cABN accurately computed the capacity for successful induction of pluripotent stem cells (iPSC) for all 9 combinations from the literature[15,18,19,22,56] (Fig. 7a). In each case, we assume a starting state in which all components are inactive, except those factors that are in the reprogramming cocktail. With the availability of published data, we next compared the relative efficiency of four factor combinations[22,24,25,29], by identifying the number of regulation steps required to stabilise in the naïve state (Fig. 7b). The cABN accurately predicted that the addition of Nanog or Tbx3 would enhance the reprogramming efficiency of Oct4/Sox2/Klf4 alone[21,5], but also that Oct4/Sox2/Klf2 would be more potent than Oct4/Sox2/Klf4[24,25]. Together, these results indicate that the 0.76 cABN is consistent with naïve pluripotency induction from somatic cells.

The 0.76 cABN could also predict the dynamics of gene activation by computing the number of steps required for each component of our network to be stably activated. Compared with gene expression measurements both at population and single-cell level from two independent studies[16,17], the program correctly identified early (Tfcp2l1 and Sall4) and late (Nanog and Esrrb) activating factors in MEF reprogramming (Fig. 7c). The predicted sequential activation between gene pairs was validated by comparing the proportion of cells expressing individual genes at different stages of reprogramming[16] at single cell resolution (Fig. 7d).

These analyses are consistent with the common gene regulatory program for naïve state maintenance and resetting governing reprogramming from somatic cells.

Discussion

In this study we implemented a combined computational and experimental approach to investigate how resetting to the naïve state is achieved. Specifically, we used automated reasoning over logical models of interaction networks[15] to derive a biological program that is consistent with the observed behaviour of resetting from primed to naïve pluripotency. The power of our iterative approach was demonstrated by an increase both in the number of predictions made as the program was refined, as well as predictive accuracy, while ensuring consistency with an increasing number of observed experimental behaviours (Fig. 6g). The biological program can predict accurately the sequence of network component activation, and also identify those component(s) that are crucial in executing the process of resetting. Since it is also constrained against functional properties of self-renewing mouse ESCs, we conclude that maintenance and induction of the naïve pluripotency state are under the control of the same core gene regulatory network. Significantly, however, we could identify TFs required selectively only during resetting.

Initially we investigated how forced expression of individual network components influences resetting. The computational approach forecast correctly that only some TFs - Klf2/4, Esrrb and Tbx3 – strongly enhance resetting. We then sought pairs of factors that act synergistically, and found that co-expression of Esrrb and Klf4 potently activate the naïve network. In this

highly efficient resetting context, we dissected the sequence of gene activation at the single cell level. A survey for components required for resetting unexpectedly identified Klf2, but not Klf4. Yet Klf2 becomes dispensable after the naïve network is established due to functional redundancy with Klf4. We conclude that resetting is a conditional process that is highly dependent on the sequence of gene activation, whereas the maintenance circuitry is robust due to layers of redundancy that confer network resilience[58].

An often overlooked aspect of modelling is the insight to be gained from analysing incorrect predictions. The distinction between Klf2 and Klf4, which are both members of the Krüppel-like family of TFs, and share high sequence homology in the DNA binding domain, was neither predicted nor intuitive. In both naïve state maintenance and somatic cell reprogramming, these two genes have been shown to have largely redundant function[25,54,55]. Furthermore, expression of Klf2 and Klf4 has a similar and potent effect on EpiSC resetting. However, genetic inactivation experiments showed that only Klf2 is required for transgene-free resetting. This can be understood in the context of network topology by examination of the kinetics of gene activation. Klf2 is up-regulated within the first 2h of resetting, whereas Klf4 becomes stably expressed only after 48h. Thus, inactivation of Klf2 leaves the cell devoid of both Klf factors for the first 2 days. Associated with this, “late” markers are not induced and resetting does not proceed. Inactivation of Klf4, in contrast, can be compensated for by the presence of Klf2, which is activated early and maintained throughout. The functional redundancy between Klf2 and Klf4 is made manifest by the observation that *Klf2* KO cells can be reset by transient expression of either Klf2 or Klf4.

It is currently debated whether acquisition of naïve pluripotency is an ordered process, following a precise sequence of events, or a stochastic system in which each cell follows a different trajectory. Our results suggest that EpiSC resetting is not stochastic, given that the biological program we have derived, which operates under a deterministic update scheme, is consistent with 176 experimental observations (accurately predicting the sequence of activation and the effect of individual genes). Based on these analyses, we propose that resetting of GOF18 EpiSCs to naïve pluripotency in 2i+LIF proceeds according to the following principles (Fig. 6g):

i. Switching culture medium from A/F to 2i+LIF leads to rapid up-regulation of some naïve factors, such as Tfcp2l1 and Klf2.
ii. Other components are sequentially activated, until the full naïve network is established. Induction of Klf4, Esrrb and Tbx3 occurs late during this process.
iii. There is a direct correlation between the timing of activation and the potency of forced expression, with “late” factors being those most able to enhance resetting.
iv. Dual expression of late factors synergistically enhances the efficiency of resetting.

Importantly, EpiSCs that do not exhibit elevated LIF-responsiveness and spontaneous resetting like the GOF18 line, also reset efficiently in response to transient expression of “late factors”. We surmise that “late factors” are necessary to consolidate the naïve network, and that their activation is therefore rate-determining.

These findings are in line with previous work suggesting that the final steps of somatic cell reprogramming follow a hierarchical, or deterministic, sequence of gene activation[16,17]. We have demonstrated that the network program derived from naïve state maintenance and

resetting has both explanatory and predictive power in somatic cell reprogramming. This further suggests that the late phase of somatic cell reprogramming is deterministic, but also highlights that a common network logic governs acquisition of naïve pluripotency from different starting cell types, either somatic or primed pluripotent stem cells. In somatic cell reprograming, several groups have described an intermediate population called pre-induced pluripotent stem cells iPSCs (pre-iPSCs)[20,26,59]. These cells lack the core naïve TF network but can be further reprogrammed to the naïve state by reducing epigenetic barriers, elevating expression of reprogramming factors and/or switching to 2i+LIF. Further comparisons of the network activation dynamics between the late phases of somatic cell reprogramming from pre-iPS cells and EpiSCs may be instructive in revealing common and unique features.

In summary, our analyses point to a common biological program that governs naïve pluripotency maintenance and induction. The power and utility of the combined computational and experimental methodology is exemplified by predicting the sequence of gene activation that occurs during resetting, and pinpointing which factors affect resetting efficiency. This method enabled the identification of pairs of TFs that dramatically accelerate resetting, yielding an overall efficiency increase of up to 50-fold. The refined cABN model set provides a platform for revealing principles of network dynamics underlying pluripotency transitions, including the emergence and dissolution of naïve pluripotency in the embryo[7]. Moreover, a similar iterative methodology using the RE:IN tool[15] could also be applied to study direct lineage reprogramming[60–62]. We also envisage that our approach could be applied to derive an understanding of network architecture and dynamics underpinning other cell fate transitions.

Author Contributions

S-J.D. carried out the computational modelling. M.A.L., E.C. and G.M. carried out the experiments. S-J.D., M.A.L. and G.M. analysed computational predictions and experimental data. S-J.D., M.A.L., G.M., and A.S. designed the study and wrote the paper. A.S. and G.M. supervised the study.

Acknowledgements

We thank members of the Smith and Martello laboratories, and Boyan Yordanov and Christoph Wintersteiger from Microsoft Research for advice and discussion. We are grateful to Jose Silva, Sirio Dupont, Michelangelo Cordenonsi and Marco Montagner for critical reading of the manuscript. We thank Yossi Buganim for providing single cell qRT-PCR data. We thank Ge Guo for providing plasmid constructs, Sarah Gharbi and Anzy Miller for their assistance with the OpenArray system. We also thank Andy Riddell for assistance for FACs sorting. S-J.D. is supported by Microsoft Research. G.M.'s laboratory is supported by grants from Giovanni Armenise-Harvard Foundation and Telethon Foundation (TCP13013). The Cambridge Stem Cell Institute receives core funding from the Wellcome Trust and Medical Research Council. M.A.L. is a Sir Henry Wellcome Postdoctoral fellow. AS is a medical research professor.

References

1. Graf, T. & Enver, T. Forcing cells to change lineages. *Nature* **462,** 587–594 (2009).
2. Cahan, P. *et al.* CellNet: Network Biology Applied to Stem Cell Engineering. *Cell* **158,** 903–915 (2014).
3. Radley, A. H. *et al.* Assessment of engineered cells using CellNet and RNA-seq. *Nat. Protoc.* **12,** 1089–1102 (2017).
4. Rackham, O. J. L. *et al.* A predictive computational framework for direct reprogramming between human cell types. *Nat. Genet.* 1–8 (2016). doi:10.1038/ng.3487
5. Takahashi, K. & Yamanaka, S. Induction of pluripotent stem cells from mouse embryonic and adult fibroblast cultures by defined factors. *Cell* **126,** 663–76 (2006).
6. Nichols, J. & Smith, A. Naive and primed pluripotent states. *Cell Stem Cell* **4,** 487–92 (2009).
7. Boroviak, T. *et al.* Lineage-Specific Profiling Delineates the Emergence and Progression of Naive Pluripotency in Mammalian Embryogenesis. *Dev. Cell* **35,** 366–382 (2015).
8. Chen, X. *et al.* Integration of external signaling pathways with the core transcriptional network in embryonic stem cells. *Cell* **133,** 1106–17 (2008).
9. Dunn, S.-J., Martello, G., Yordanov, B., Emmott, S. & Smith, A. G. Defining an essential transcription factor program for naive pluripotency. *Science (80-.).* **344,** 1156–1160 (2014).
10. Herberg, M. & Roeder, I. Computational modelling of embryonic stem-cell fate control. *Development* **142,** 2250–60 (2015).
11. MacArthur, B. D. *et al.* Nanog-dependent feedback loops regulate murine embryonic stem cell heterogeneity. *Nat. Cell Biol.* **14,** 1139–47 (2012).
12. Niwa, H., Ogawa, K., Shimosato, D. & Adachi, K. A parallel circuit of LIF signalling pathways maintains pluripotency of mouse ES cells. *Nature* **460,** 118–22 (2009).
13. Rue, P. & Martinez Arias, A. Cell dynamics and gene expression control in tissue homeostasis and development. *Mol. Syst. Biol.* **11,** 792–792 (2015).
14. Yachie-Kinoshita, Ayako Onishi, K., Ostblom, J., Posfai, E., Rossant, J. & Zandstra, P. W. Modeling Signaling-Dependent Pluripotent Cell States With Boolean Logic Can Predict Cell Fate Transitions. *biorXiv* (2017). doi:10.1101/115683
15. Yordanov, B. *et al.* A method to identify and analyze biological programs through automated reasoning. *npj Syst. Biol. Appl.* **2,** 16010 (2016).
16. Buganim, Y. *et al.* Single-cell expression analyses during cellular reprogramming reveal an early stochastic and a late hierarchic phase. *Cell* **150,** 1209–22 (2012).
17. O'Malley, J. *et al.* High-resolution analysis with novel cell-surface markers identifies routes to iPS cells. *Nature* **499,** 88–91 (2013).
18. Stuart, H. T. *et al.* NANOG Amplifies STAT3 Activation and They Synergistically Induce the Naive Pluripotent Program. *Curr. Biol.* **24,** 340–346 (2014).
19. Tang, Y. *et al.* Jak/Stat3 signaling promotes somatic cell reprogramming by epigenetic regulation. *Stem Cells* **30,** 2645–2656 (2012).

20. Silva, J. *et al.* Promotion of Reprogramming to Ground State Pluripotency by Signal Inhibition. *PLoS Biol.* **6,** e253 (2008).

21. Han, D. W. *et al.* Epiblast Stem Cell Subpopulations Represent Mouse Embryos of Distinct Pregastrulation Stages. *Cell* **143,** 617–627 (2010).

22. Hanna, J. *et al.* Direct cell reprogramming is a stochastic process amenable to acceleration. *Nature* **462,** 595–601 (2009).

23. Sone, M. *et al.* Hybrid Cellular Metabolism Coordinated by Zic3 and Esrrb Synergistically Enhances Induction of Naive Pluripotency. *Cell Metab.* **25,** 1103–1117.e6 (2017).

24. Feng, B. *et al.* Reprogramming of fibroblasts into induced pluripotent stem cells with orphan nuclear receptor Esrrb. *Nat. Cell Biol.* **11,** 197–203 (2009).

25. Nakagawa, M. *et al.* Generation of induced pluripotent stem cells without Myc from mouse and human fibroblasts. *Nat. Biotechnol.* **26,** 101–106 (2007).

26. Mikkelsen, T. S. *et al.* Dissecting direct reprogramming through integrative genomic analysis. *Nature* **454,** 49–55 (2008).

27. Samavarchi-Tehrani, P. *et al.* Functional Genomics Reveals a BMP-Driven Mesenchymal-to-Epithelial Transition in the Initiation of Somatic Cell Reprogramming. *Cell Stem Cell* **7,** 64–77 (2010).

28. Tanabe, K., Nakamura, M., Narita, M., Takahashi, K. & Yamanaka, S. Maturation, not initiation, is the major roadblock during reprogramming toward pluripotency from human fibroblasts. *Proc. Natl. Acad. Sci.* **110,** 12172–12179 (2013).

29. Han, J. *et al.* Tbx3 improves the germ-line competency of induced pluripotent stem cells. *Nature* **463,** 1096–1100 (2010).

30. Golipour, A. *et al.* A Late Transition in Somatic Cell Reprogramming Requires Regulators Distinct from the Pluripotency Network. *Cell Stem Cell* **11,** 769–782 (2012).

31. Di Stefano, B. *et al.* C/EBPα poises B cells for rapid reprogramming into induced pluripotent stem cells. *Nature* **506,** 235–239 (2013).

32. Di Stefano, B. *et al.* C/EBPα creates elite cells for iPSC reprogramming by upregulating Klf4 and increasing the levels of Lsd1 and Brd4. *Nat. Cell Biol.* **18,** 371–381 (2016).

33. Silva, J. *et al.* Nanog is the gateway to the pluripotent ground state. *Cell* **138,** 722–37 (2009).

34. Guo, G. *et al.* Klf4 reverts developmentally programmed restriction of ground state pluripotency. *Development* **136,** 1063–1069 (2009).

35. Tsakiridis, A. *et al.* Distinct Wnt-driven primitive streak-like populations reflect in vivo lineage precursors. *Development* **141,** 1209–1221 (2014).

36. Kojima, Y. *et al.* The Transcriptional and Functional Properties of Mouse Epiblast Stem Cells Resemble the Anterior Primitive Streak. *Cell Stem Cell* **14,** 107–120 (2014).

37. Brons, I. G. M. *et al.* Derivation of pluripotent epiblast stem cells from mammalian embryos. *Nature* **448,** 191–195 (2007).

38. Tesar, P. J. *et al.* New cell lines from mouse epiblast share defining features with human embryonic stem cells. *Nature* **448,** 196–199 (2007).

39. Festuccia, N. *et al.* Esrrb Is a Direct Nanog Target Gene that Can Substitute for Nanog

Function in Pluripotent Cells. *Cell Stem Cell* **11,** 477–490 (2012).

40. Gillich, A. *et al.* Epiblast Stem Cell-Based System Reveals Reprogramming Synergy of Germline Factors. *Cell Stem Cell* **10,** 425–439 (2012).

41. Hall, J. *et al.* Oct4 and LIF/Stat3 additively induce Krüppel factors to sustain embryonic stem cell self-renewal. *Cell Stem Cell* **5,** 597–609 (2009).

42. Martello, G., Bertone, P. & Smith, A. Identification of the missing pluripotency mediator downstream of leukaemia inhibitory factor. *EMBO J.* 1–14 (2013). doi:10.1038/emboj.2013.177

43. Bernemann, C. *et al.* Distinct Developmental Ground States of Epiblast Stem Cell Lines Determine Different Pluripotency Features. *Stem Cells* **29,** 1496–1503 (2011).

44. Yang, J. *et al.* Stat3 Activation Is Limiting for Reprogramming to Ground State Pluripotency. *Cell Stem Cell* **7,** 319–328 (2010).

45. Ying, Q.-L. *et al.* The ground state of embryonic stem cell self-renewal. *Nature* **453,** 519–23 (2008).

46. Qiu, D. *et al.* Klf2 and Tfcp2l1, Two Wnt/β-Catenin Targets, Act Synergistically to Induce and Maintain Naive Pluripotency. *Stem Cell Reports* **5,** 314–322 (2015).

47. Martello, G. *et al.* Esrrb is a pivotal target of the Gsk3/Tcf3 axis regulating embryonic stem cell self-renewal. *Cell Stem Cell* **11,** 491–504 (2012).

48. Ye, S., Li, P., Tong, C. & Ying, Q.-L. Embryonic stem cell self-renewal pathways converge on the transcription factor Tfcp2l1. *EMBO J.* **32,** 2548–2560 (2013).

49. Kalkan, T. *et al.* Tracking the embryonic stem cell transition from ground state pluripotency. *Development* dev.142711 (2017). doi:10.1242/dev.142711

50. Acampora, D. *et al.* Loss of the Otx2-Binding Site in the Nanog Promoter Affects the Integrity of Embryonic Stem Cell Subtypes and Specification of Inner Cell Mass-Derived Epiblast. *Cell Rep.* **15,** 2651–2664 (2016).

51. Anchang, B. *et al.* Visualization and cellular hierarchy inference of single-cell data using SPADE. *Nat. Protoc.* **11,** 1264–1279 (2016).

52. Qiu, P. *et al.* Extracting a cellular hierarchy from high-dimensional cytometry data with SPADE. *Nat. Biotechnol.* **29,** 886–891 (2011).

53. Guo, G. & Smith, A. A genome-wide screen in EpiSCs identifies Nr5a nuclear receptors as potent inducers of ground state pluripotency. *Development* **3192,** 3185–3192 (2010).

54. Jiang, J. *et al.* A core Klf circuitry regulates self-renewal of embryonic stem cells. *Nat. Cell Biol.* **10,** 353–360 (2008).

55. Yeo, J.-C. *et al.* Klf2 Is an Essential Factor that Sustains Ground State Pluripotency. *Cell Stem Cell* **14,** 864–872 (2014).

56. Sanchez-Castillo, M. *et al.* CODEX: a next-generation sequencing experiment database for the haematopoietic and embryonic stem cell communities. *Nucleic Acids Res.* **43,** D1117–D1123 (2015).

57. Takahashi, K. & Yamanaka, S. Induction of pluripotent stem cells from mouse embryonic and adult fibroblast cultures by defined factors. *Cell* **126,** 663–76 (2006).

58. Martello, G. & Smith, A. The Nature of Embryonic Stem Cells. *Annu. Rev. Cell Dev. Biol.* **30,** 647–675 (2014).

59. Chen, J. *et al.* H3K9 methylation is a barrier during somatic cell reprogramming into iPSCs. *Nat. Genet.* **45,** 34–42 (2012).

60. Xie, H., Ye, M., Feng, R. & Graf, T. Stepwise Reprogramming of B Cells into Macrophages. *Cell* **117,** 663–676 (2004).

61. Vierbuchen, T. *et al.* Direct conversion of fibroblasts to functional neurons by defined factors. *Nature* **463,** 1035–1041 (2010).

62. Davis, R. L., Weintraub, H. & Lassar, A. B. Expression of a single transfected cDNA converts fibroblasts to myoblasts. *Cell* **51,** 987–1000 (1987).

Materials and Methods

Cell lines

All EpiSC lines in this work were cultured as described in [34] on fibronectin-coated plates in serum-free media N2B27 (DMEM/F12 and Neurobasal [both Life Technologies] in 1:1 ratio, with 0.1 mM 2-mercaptoethanol, 2 mM L-glutamine, 1:200 N2 [Life Technologies], and 1:100 B27 [Life Technologies]) supplemented with FGF2 (12 ng/ml) and Activin (20 ng/ml) produced in house. GOF18 EpiSCs were described in [21] and generously provided by Hans Schöler. OEC2-Y118F (Oct4-GFP) EpiSCs are described in Yang et al (2010). OGRK cells were derived from E5.5 post-implantation mouse embryo using N2B27 medium supplemented with 20 ng/ml Activin A and 12 ng/ml Fgf2 together with 2 µM XAV939 (Sigma Aldrich, X3004).

Plasmid constructions

Individual core pluripotency network factors were either amplified from cDNA or cloned from existing expression plasmids into pENTR2B donor vector. Subsequently the transgenes were gateway cloned into the same destination vector containing PB-CAG-DEST-bghpA and pGK-Hygro selection cassette. The sizes of final expression constructs range from 8.5kb to 10.7kb.

To construct the T2A linked inducible overexpression plasmids, Esrrb and either Tbx3 or Klf4 were PCR amplified with part of the T2A sequence flanking the 3' or 5' of the gene respectively. Three-way ligation of both gene fragments together with pENTR2B vector resulted in the fusion of EsrrbT2ATbx3 or EsrrbT2AKlf4. Subsequently the fusion constructs were gateway cloned into the same final destination vector containing TRE-CMV and a Venus reporter. To generate co-expression cell lines, cells were co-transfected with a plasmid containing rtTA and a Neomycin selection cassette.

Transient overexpression of factors for EpiSC resetting

1.5µg of plasmid DNA was transfected with 3µl of Lipofectamine2000 to 1x105 EpiSCs in suspension in Fgf2/ActivinA (F/A) containing N2B27 medium with Rock inhibitor Y-27632 (Sigma, 1:1000) overnight in one well of the 12 well plate. The next day, medium was switched to 2i/LIF medium to initiate reprogramming. GFP positive colonies were scored at day 7 of reprogramming. When a combination of two factors were co-transfected, 0.75µg of plasmid DNA of each factor were used. For the control single factor transfections, 0.75 µg of plasmid DNA harbouring the indicated factor together with 0.75µg of empty vector plasmid were used.

Generation of KO EpiSCs with CRISPR/Cas9

The gRNA pair were chosen to delete the largest coding exons within Klf2 and Klf4 to ensure the complete loss of function. The gRNA design was conducted using online CRISPR gRNA design tool https://www.dna20.com/eCommerce/cas9/input. The chosen gRNAs were based on the minimal off-target scores. The gRNA containing plasmids were cloned by annealing the complementary oligos indicated in Table S7, and cloned into BbsI digested pX458 vector (Addgene). The constructs were sequence validated before transfection.

A pair of gRNA containing plasmids based on px458 designed with specific deletion were transfected using Lipofectamine2000 (Invitrogen). 500 ng of each plasmid were transfected with 3 ul Lipofectamine2000 to 2x105 EpiSCs in suspension in Activin/Fgf2/Xav containing N2B27 medium with Rock inhibitor Y-27632 (Sigma, 1:1000) overnight in one well of the 12 well plate. The next day, the media was refreshed with Activin/Fgf2/Xav/Rock inhibitor and 48 hours post transfection, 2,000 GFP high cells were sorted into 6 cells for colony formation. Individual colonies were picked and genotyping was conducted from extracted genomic DNA by primers indicated in Table S7 to identify clones with designed deletion. For Klf2 KO, deletion from both gRNAs resulted in genotyping PCR product to shift from 890 bp representing the wild type allele to 130 bp. For Klf4 KO, deletion from both gRNAs resulted in genotyping PCR product to shift from 840 bp representing the wild type allele to 100 bp. Only homozygous mutants were chosen for subsequent experiment.

siRNA knockdown for EpiSC resetting

Final concentration of 20nM siRNAs together with 0.5 µl of Dharmafect 1 (Dharmacon, T-2001-01) was transfected to 1x105 EpiSCs in suspension in Activin/Fgf2 containing N2B27 medium with Rock inhibitor Y-27632 (Sigma, 1:1000) overnight in one well of the 12 well plate. At least 2 siRNAs were used for each target gene knockdown and the catalogue number of all siRNAs are shown in Table S5. The next day, medium was switched to 2i/LIF medium to initiate reprogramming. GFP positive colonies were scored at day 7 of reprogramming.

siRNA knockdown for ESC maintenance

To test the effect of knock down of individual factors on maintenance of pluripotency we transfected siRNA in mES cells and replated them after 48h at clonal density, as described in [9]. 5 Days after plating we scored the number of pluripotent colonies, relative to cell transfected with a control siRNA. At least 2 siRNAs were used for each target gene knockdown and the catalogue number of all siRNAs are shown in Table S5.

EpiSC resetting of DOX inducible factor combinations

Cells with the stably integrated piggyBac transposase (500ng), piggybac constructs harbouring the DOX inducible factor combinations (375ng) and rTtA construct (125ng) were plated in N2B27 medium containing F/A. The next day, medium was switched to 2i+LIF with or without DOX 0.2µg/ml to for 2 days to induce transgene expression. At day 2 medium was switched to 2i + LIF. Images were acquired at day 6 and clonal assays were performed at day 2-6-8. (See also Fig. 3d). For single cell qPCR analysis of resetting intermediates, cells were kept in 2i+LIF+DOX throughout the experiment for up to 4 days. Clonal assay was performed by replating 250 cells in a well of a 12 well plate in 2i+LIF without DOX.

Alkaline Phosphatase staining

For AP staining, cells were fixed with a citrate–acetone– formaldehyde solution and stained using the Alkaline Phosphatase kit (Sigma, cat. 86R-1KT). Plates were scanned using a Nikon Scanner and scored manually.

RNA extraction, reverse transcription and Real-time PCR

Total RNA was isolated using RNeasy kit (Qiagen) and DNase treatment was conducted either after RNA purification or during column purification. cDNA was transcribed from 0.5~1 ug

RNA using SuperScriptIII (Invitrogen) and oligo-dT priming. Real-time PCR was performed using on StepOnePlus and QuantStudio machines (Applied Biosystems) with Fast Sybr green master mix (Applied Biosystems). Target gene primer sequences and probes used are listed in Tables S6. Expression levels were normalised to Actinβ or Gapdh. Technical replicates for at least two independent experiments were conducted. The results were shown as mean and standard deviation calculated by StepOnePlus software (Applied Biosystems).

Single cell gene expression profiling

OpenArrays were custom designed by ThermoFisher with the Taqman assay ID shown in Table S8. Single cells were directly deposited by Fluorescence Activated Cell Sorting into 9µl of a pre-amplification mixture (CellDirect One-Step qRT-PCR kit, 11753-500) which contains 0.05x of each TaqMan assay, 1x CellDirect reaction mix, 200 ng/µl SuperscriptIII/Platinum Taq, 100 ng/µl SUPERRase-In (ThermoFisher) in DNA suspension buffer (TEKnova). The reverse transcription and gene specific PCR amplification was carried out in a thermal cycler with the following condition: 50°C for 30min, 95°C for 2 min followed by 24 cycles of 95°C for 15 sec, 60°C for 4 min. cDNA was diluted 1:10 and only cells with at least two housekeeping genes amplified were chosen for whole panel gene expression profiling. The cDNA samples were loaded onto an OpenArray using OpenArray AccuFill system and the quantitative real-time PCR was run using Quantstudio 12K Flex System. For gene expression analysis, the average of five all housekeeping genes (Actβ, Gapdh, Tbp, Ppia, Atp5a1) were used for normalisation.

Identifying Possible Interactions

The initial 0.832 ABN was constructed from a set of *definite* interactions downstream of LIF, CH and PD, based on previous experimental studies that identified the direct targets of these signals [12,33,42,46,47], and a set of *possible* interactions derived from our RNA-Seq and RT-qPCR datasets as follows.

Seven Pearson coefficients were generated for each gene pair, one from each dataset, which quantify the correlation in gene expression under the action of different combinations of LIF, CH and PD. An interaction between two genes was defined to be possible and positive if at least one of these coefficients was above a given threshold, and the majority of the remaining coefficients were greater than zero. Similarly, an interaction between two genes was defined to be possible and negative if at least one of these coefficients was below the negative of a given threshold, and the majority of the remaining coefficients were less than zero. In cases where there are positive coefficients above the threshold as well as negative coefficients below the threshold, we let the majority rule. Given that correlations alone do not reveal which gene behaves as the regulator, possible interactions are defined to be bidirectional.

We identified the Pearson correlation threshold by constructing a set of experimental constraints (Fig. 1c and S1d, as described below). We then sought the maximum Pearson coefficient threshold that generated a set of possible interactions that could satisfy these expected behaviours. In doing so, we minimised the number of possible interactions, and therefore the number of concrete models in the ABN.

Discretising Gene Expression Measurements and Encoding Experimental Observations

We discretised the gene expression profile of GOF18 EpiSCs (Fig. S1d, top) by setting a gene to High if its expression was at least 0.5 of its level in mouse ESCs in 2i+LIF. We therefore

discretised the GOF18 EpiSC state to be such that Oct4, Sox2 and Sall4 were High, while the remaining TFs were Low. MEK/ERK and Tcf3 were also set to High in these cells, as they are cultured in F/A.

We added a set of experimental observations to our existing set of constraints concerning maintenance of pluripotency [9], by discretising gene expression profiles for the following experimental behaviours, shown in Fig. S1d (bottom) and summarised in the Supplementary File, 'SupplementalFileAllConstraintsImposed.xlsx':

Control: If none of the pluripotency factors are initially expressed, then 2i+LIF alone is insufficient to reach the naïve state, which is defined to be the gene expression state of mouse ESCs cultured in 2i+LIF[9].

EpiSC in 2i+LIF: Starting from the discretised gene expression profile of GOF18 EpiSCs, 2i+LIF is sufficient for these cells to reset and stabilise in the naïve state[21,42].

EpiSC in 2i only: 2i alone is insufficient to reset GOF18 EpiSCs, and so we constrain the networks by excluding trajectories that reach this state under 2i[42].

EpiSC in 2i with Tfcp2l1 expression: Forced expression of Tfcp2l1 is sufficient to reset GOF18 EpiSCs in 2i alone[42].

Nanog knockout EpiSCs in 2i+LIF: Knocking out Nanog prevents EpiSCs from reaching the naïve state in 2i+LIF[18].

Nanog knockout EpiSCs in LIF+CH: Nanog knockout EpiSCs in the presence of LIF+CH is sufficient to activate Oct4, Esrrb, Klf2, Tfcp2l1, Klf4 and Stat3[18].

Each constraint consists of an initial and final discrete gene expression pattern, which are defined at specific steps along the network trajectory. We allow 20 steps for each experiment trajectory to stabilise. The final state is either unreachable (indicated by a bar over the final time step in Fig. S1d), or stable (indicated by an asterisk). In the case where the full gene expression state cannot be defined (e.g. Tfcp2l1 forced expression in 2i) then we define the final state at two sequential steps to ensure that the key genes are sustained.

We encoded these constraints together with the ABN into the RE:IN tool. The discrete gene expression profiles are imposed as initial and final states of trajectories that network models must satisfy. RE:IN synthesises only those concrete network models consistent with this set of expected behaviours, which comprise the cABN.

When investigating the gene activation kinetics of resetting, we included the observation that forced expression of Sall4 in GOF18 EpiSCs does not increase the efficiency of resetting to the naïve state (Fig. 1f). To ensure that this holds for all models, we encoded a new constraint that defined when Sall4 expression is imposed, an EpiSC will not reach the naïve state at an earlier step than the case in which it is not, regardless of the step at which the latter occurs. This is illustrated in the Supplemental File that describes all constraints. Similarly, the constraint we added concerning Klf4 knockout in EpiSC resetting is described in the same file.

Network Dynamics

Each concrete network model in the ABN is considered as a state transition system, with a deterministic update scheme. Dynamic behaviour emerges from the update functions that are applied to each component, which are logical functions that define how the gene updates its state in response to its regulators. Often such update functions are defined according to the named regulators of a given target, but given that we have an ABN, the regulators of a target can vary between concrete models. We therefore defined a set of twenty update functions that are not dependent on named regulators [15], which reason about whether some, all or none of a targets activators/repressors are present. In this present study, we consider a subset of these conditions (regulation conditions 0-8 as described in [15]), which assume that a gene requires at least one activator in order to be expressed. In a concrete model, each component is assigned one of these regulation conditions to ensure that the constraints are met.

Required and Disallowed Interactions

We characterise the cABN by identifying which of the possible interactions are common to all concrete networks – required interactions – and which are never present – disallowed interactions. A simple algorithm is implemented that first identifies a single concrete network consistent with the experimental observations. Each of the possible interactions that are instantiated as present in this example solution are subsequently removed individually from the ABN, and RE:IN identifies whether the constraints are satisfiable in the absence of the interaction. If the constraints are unsatisfiable when a given possible interaction is removed, then it must be the case that it is present in every concrete network that satisfies the constraints. Conversely, we examine all interactions not present in the example solution that we initially found, testing whether the constraints are still satisfiable if these interactions are individually imposed as definite. If, once a possible interaction is switched to being definite and the constraints are no longer satisfiable, then we conclude that that particular interaction can never be present in any concrete model solution. The remaining interactions – those which can be removed or imposed individually without preventing the constraints from being satisfied – remain as possible, and will be needed in some concrete models, but not all.

Formulating Model Predictions

Via RE:IN, our approach automatically synthesises the entire set of models consistent with the expected behaviour of the experimental system. When we formulate predictions of untested behaviour we interrogate the entire set of consistent models, and only if they all are in agreement is a prediction generated and tested. The behaviour of only a subset of models, which may not be fully representative, is never tested experimentally.

To generate predictions, hypotheses are encoded as additional constraints, and we test whether they are satisfiable together with the set of expected behaviours. Crucially, we also test the null hypothesis – that under the same conditions the expected behaviour cannot be obtained. If both are satisfiable independently, then it must be the case that some models satisfy the hypothesis, while others satisfy the null hypothesis. If all models satisfy the hypothesis, while the null is unsatisfiable, then a prediction can be formulated based on all concrete models that the hypothesis is correct. If the null hypothesis is satisfiable, while the

hypothesis itself is unsatisfiable, then a prediction can also be made, which is that the expected behaviour is never observed.

For example, to test whether GOF18 EpiSCs can reset to the naïve state under Gbx2 knockdown in 2i+LIF, we formulate a constraint with these initial and final states. We then also formulate and test the constraint that GOF18 EpiSCs do not reach the naïve state under Gbx2 knockout in 2i+LIF. In this particular example, we found that our hypothesis constraint was satisfiable, while the null hypothesis constraint was unsatisfiable. Therefore, all concrete models predict that GOF18 EpiSCs will reset in 2i+LIF with Gbx2 knockdown, which was subsequently found to be consistent with experimental evidence.

Identifying the Number of Regulation Steps to Reach the Naïve State

To determine how many regulation steps are required to stabilise in the naïve state, starting from the EpiSC state, we formulate hypotheses for each possible case, e.g. that it stabilises at step 2, at step 3, at step 4, etc. As described above, for each case we also test the null hypothesis. In this manner, we deduced whether some, all or none of the models allowed EpiSCs to stabilise in the naïve state at a given regulation step.

K-means clustering to discretise the single cell gene expression

We used k-means clustering with k=2 on the log10-transformed single cell gene expression data (Fig. 4d) in order to discretise gene expression into High/Low, for which we identified a unique discretisation threshold for each gene. Of note, the mean expression levels in the two clusters differ by several orders of magnitude.

SPADE analysis

We conducted a SPADE analysis using SPADEV3.0 [51], using the default settings. This was carried out on the log10-transformed single cell gene expression data (Fig. 4d).

Quantification and Statistical Analysis

We used the student's t test with $p<0.05$ (paired t-test with one tail distribution) to define statistical significance. The specific details of the test, number of the experiments (n), and the dispersion and precision measurements (mean, median, standard errors and standard deviations) can be found in figure legends for Fig. 1f, S2 and 2B.

Data and Software Availability

The files used to generate the cABN will be made available at research.microsoft.com/rein, which also provides a tutorial for the tool, and FAQ. These have been made available to reviewers with this submission.

Supplemental Items

Fig. S1: (Related to Fig. 1) Deriving and constraining the 0.832 ABN.

Fig. S2: (Related to Fig. 1) Predicting the relative potency of single factor forced expression in enhancing resetting to the naïve state.

Fig. S3: (Related to Fig. 4a, b) A comparison of the resetting kinetics under empty vector control and dual factor expression, visualised on the 0.782 cABN.

Fig. S4: (Related to Fig. 3) Investigating dual factor expression in OEC2-GY118 EpiSCs.

Fig. S5: (Related to Fig. 4) Gene expression analysis of two reset clones generated by forced expression of Esrrb-T2A-Klf4 for 4 days (see Fig. 5) and cultured for 3 passages in 2i+LIF without DOX.

Fig. S6: (Related to Fig. 6) Klf2 and Klf4 KO EpiSC generation and transgene free Klf2KO iPSCs.

Table S1: (Related to Fig. 4) Single cell gene expression of ESC and EpiSC associated genes quantified by real time quantitative PCR.

Table S2: (Related to Fig. 6) The set of experimental constraints imposed on the 0.76 ABN.

Table S3: (Related to Fig. 6h) Comparison of predictions generated by 0.832, 0.782 and 0.76 cABN to the experimental observations.

Table S4: (Related to Fig. 6) Required and disallowed interactions in 0.76 cABN compared to the the CHIP-sequencing data.

Table S5: siRNAs used in this study.

Table S6: Real-time quantitative PCR primers and probes.

Table S7**:** DNA oligonucleotides used to generate gRNAs and genotype Klf2 and klf4 knockouts.

Table S8: Custom Taqman OpenArray real-time quantitative PCR IDs used for the single cell gene expression.

Figure 1

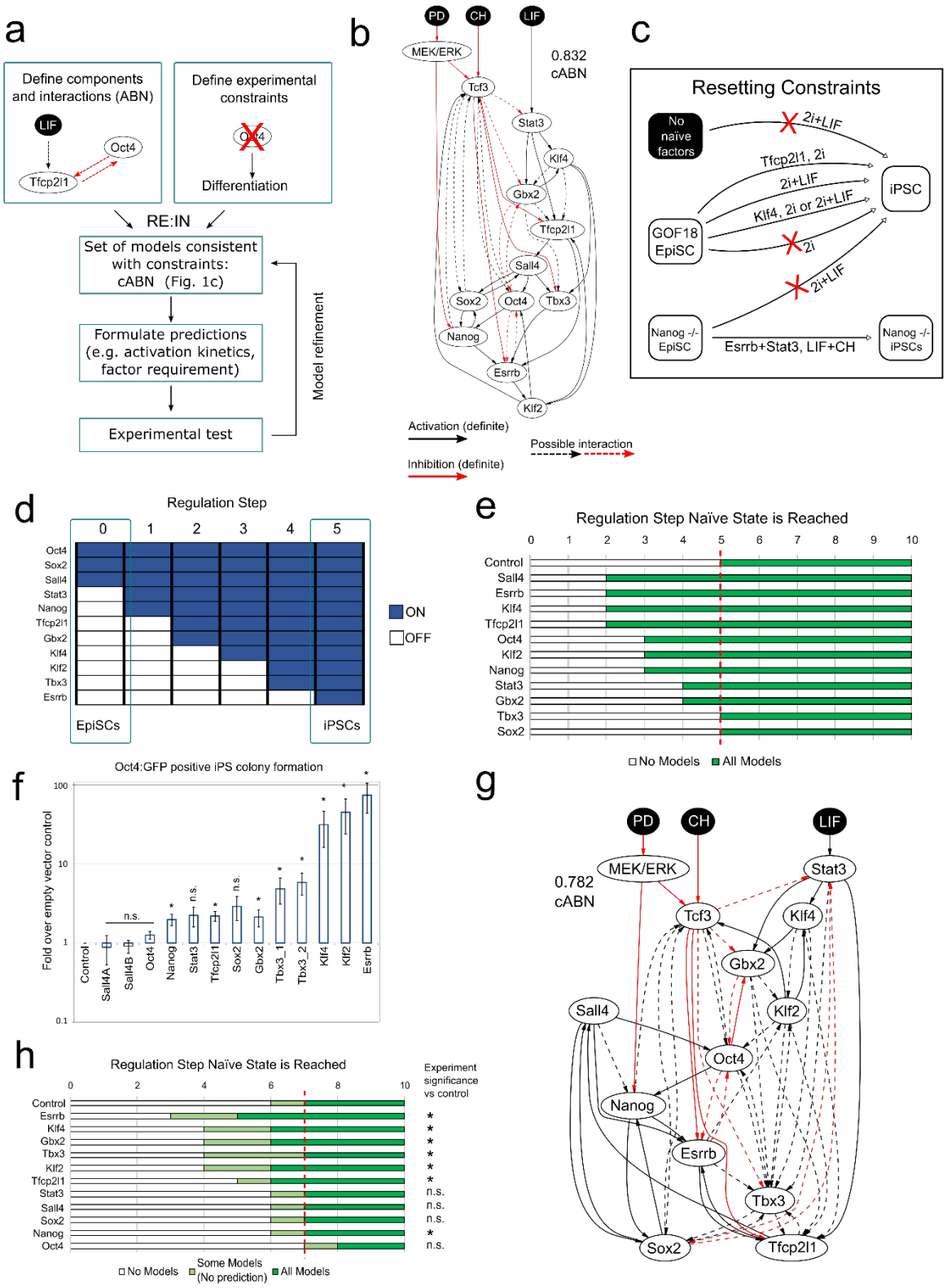

Figure 1: Network models consistent with naïve state maintenance predict the effect of TF forced expression in resetting from primed pluripotency. See also Fig. S1, S2. (a) Flow-chart describing the

methodology. Network components were identified based on functional studies from the literature, and possible interactions between components were defined based on pairwise gene expression correlation. A set of experimental results served as constraints. The software RE:IN synthesises all possible interaction networks consistent with the constraints, which is termed the cABN. The cABN is used to formulate predictions that will be tested experimentally. If predictions are falsified, the cABN can be further refined by incorporating new findings as constraints. The refined cABN is used to generate further predictions. (b) cABN derived from a Pearson coefficient threshold of 0.832, consistent with constraints previously defined for ESC self-renewal (Dunn et al. 2014). Solid arrow, required interaction; dashed arrow, possible and allowed interaction; black arrow, activation; red arrow, inhibition. (c) Illustration of the resetting constraints. (d) Example of the sequence of gene activation of naïve network components during resetting, represented by regulation steps of the network trajectory. (e) Predicted number of regulation steps required for all models to stabilise in the naïve state under forced expression of each single network component. (f) Fold increase of Oct4:GFP^{+} colony number under forced expression of individual factors over empty vector control. Mean +/- SEM, $n \geq 5$. *, $p<0.05$ Student's t-test; n.s., not significant. (g) cABN derived from a Pearson coefficient threshold of 0.782. (h) Predictions from the 0.782 cABN. Light green regions indicate where some, but not all, concrete networks allow stable conversion to the naïve state, preventing a prediction from being made. *, a significant increase over control was observed experimentally, as shown in f.

Figure 2

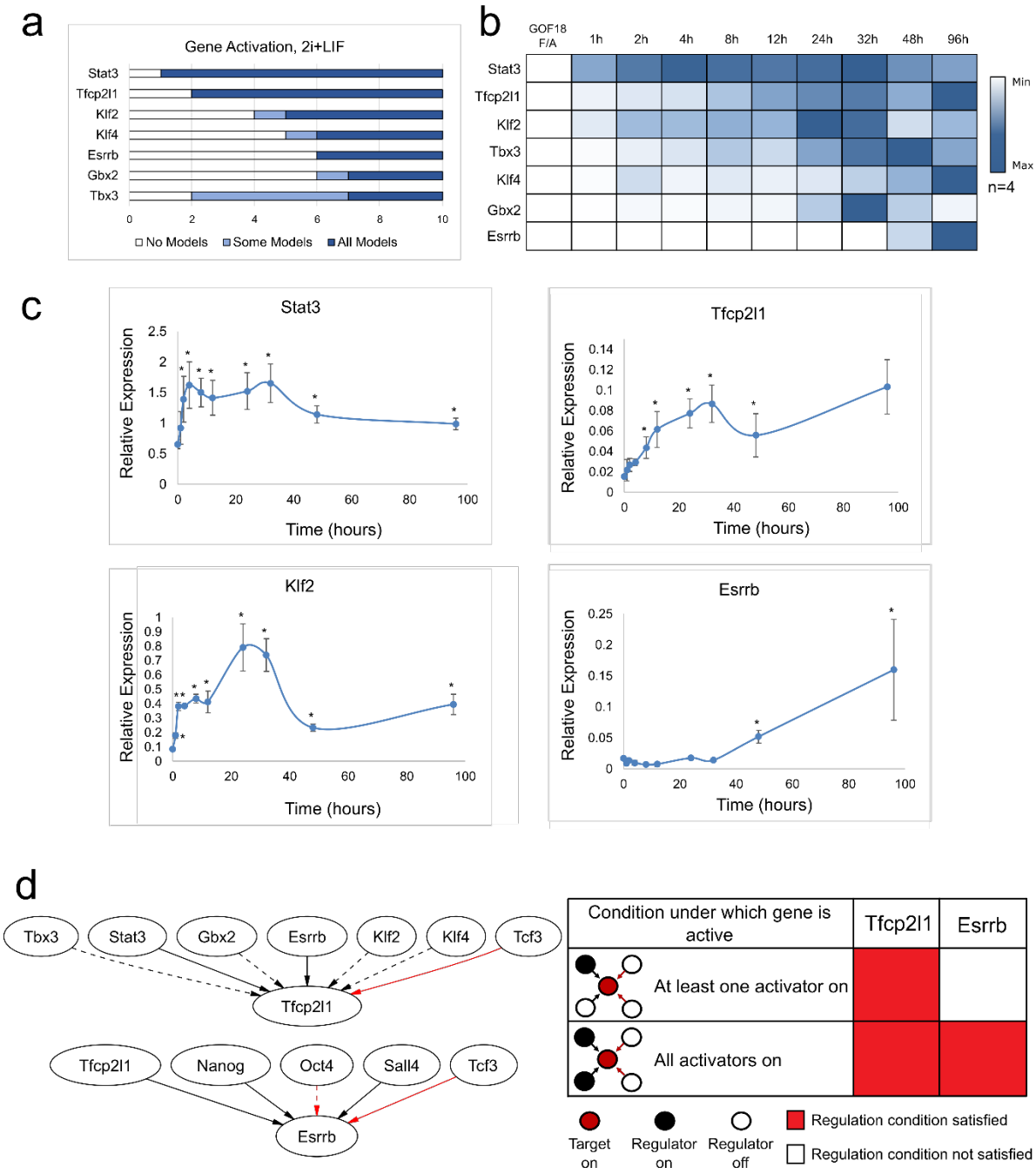

Figure 2: Models predict the sequence of gene activation of the naïve network. (a) Model predictions of the number of regulation steps required for permanent activation of gene expression of each network component. Light blue regions indicate where only some models predict the given gene has permanently activated. (b) A heatmap of the average gene expression relative to β-actin over a resetting time course in 2i+LIF. Each row is coloured according to the unique minimum and maximum for that gene. n=4. (c) Gene expression for Stat3, Klf2, Esrrb and Tfcp2l1 during EpiSC resetting relative to established mouse ESCs. Mean +/- SEM, n=4. *, Student's t-test, $p<0.05$. (d) Left: Local network

topology for Tfcp2l1 and Esrrb. Right: Summary of regulation conditions required by Tfcp2l1 and Esrrb in the 0.782 cABN.

Figure 3

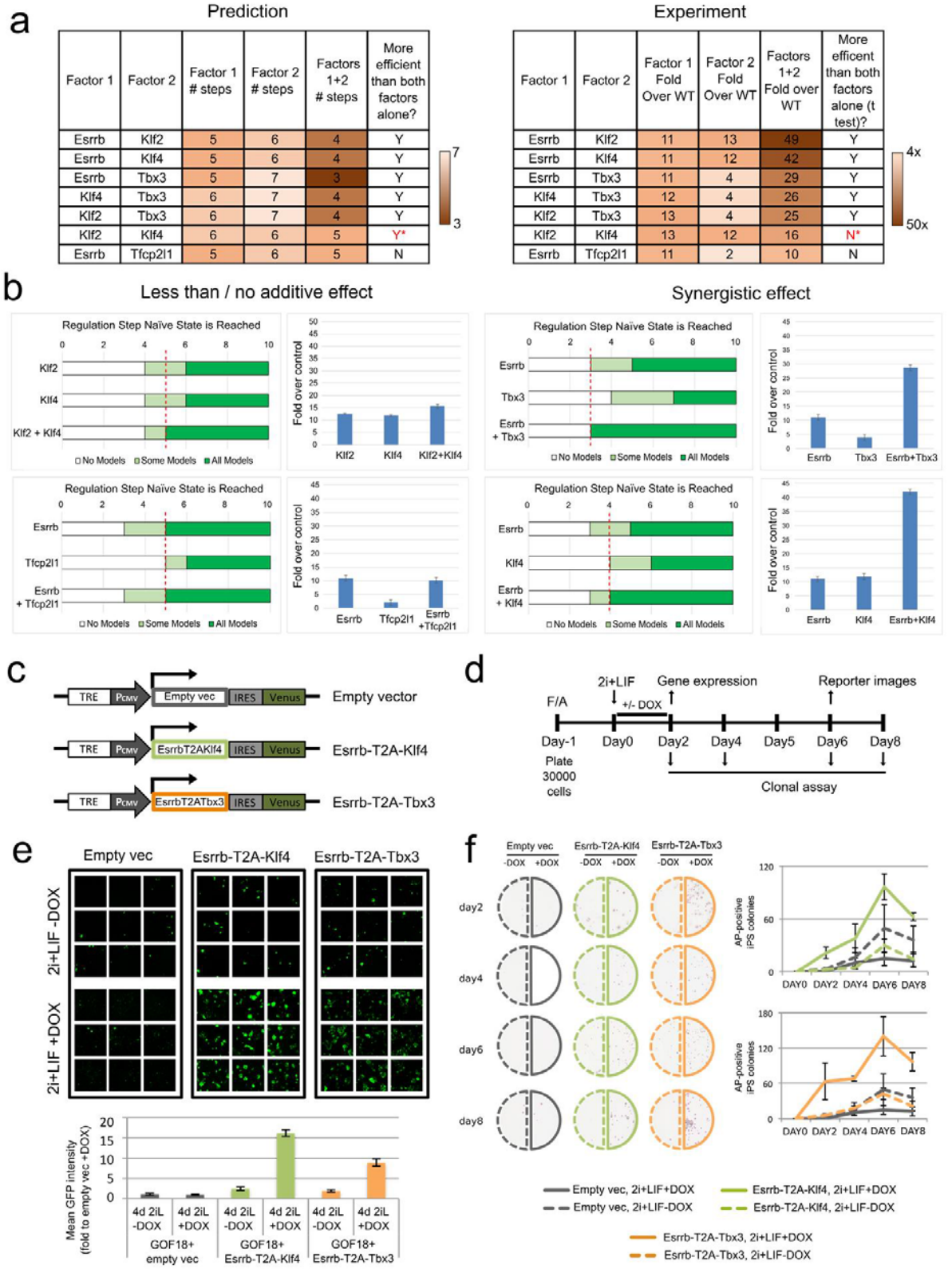

Figure 3: Combinations of late-activated factors enhance resetting by accelerating network activation. See also Fig. S4. (a) Left: Comparison of the number of steps required for all models to stabilise in the naïve state under single and dual factor expression. Right: Experimental results showing the fold increase in colony number over empty vector control, under single and dual factor expression.

Y = Yes, N = No, * = incorrect prediction. (b) Predictions and experimental validation of examples of synergistic and non-additive factor combinations. Fold increase over empty vector control of Oct4:GFP$^+$ colonies was measured experimentally. Mean +/- SD, n=2. (c) DOX inducible constructs used for co-expression experiments. (d) Experimental scheme for functional characterisation of Esrrb-T2A-Klf4 or Esrrb-T2A-Tbx3 forced expression in resetting. (e) Top: Representative confocal images of Oct4:GFP reporter expression. The indicated cell lines were treated with DOX for the first 2 days and imaged at Day 6. Bottom: Quantification of mean Oct4-GFP intensity signal shown in the top images. Mean +/- SEM, n=2. (f) Representative alkaline phosphatase (AP) staining images (left) and quantification (right) of AP$^+$ colonies after clonal assay, as described in panel D. Mean +/- SEM, n=3.

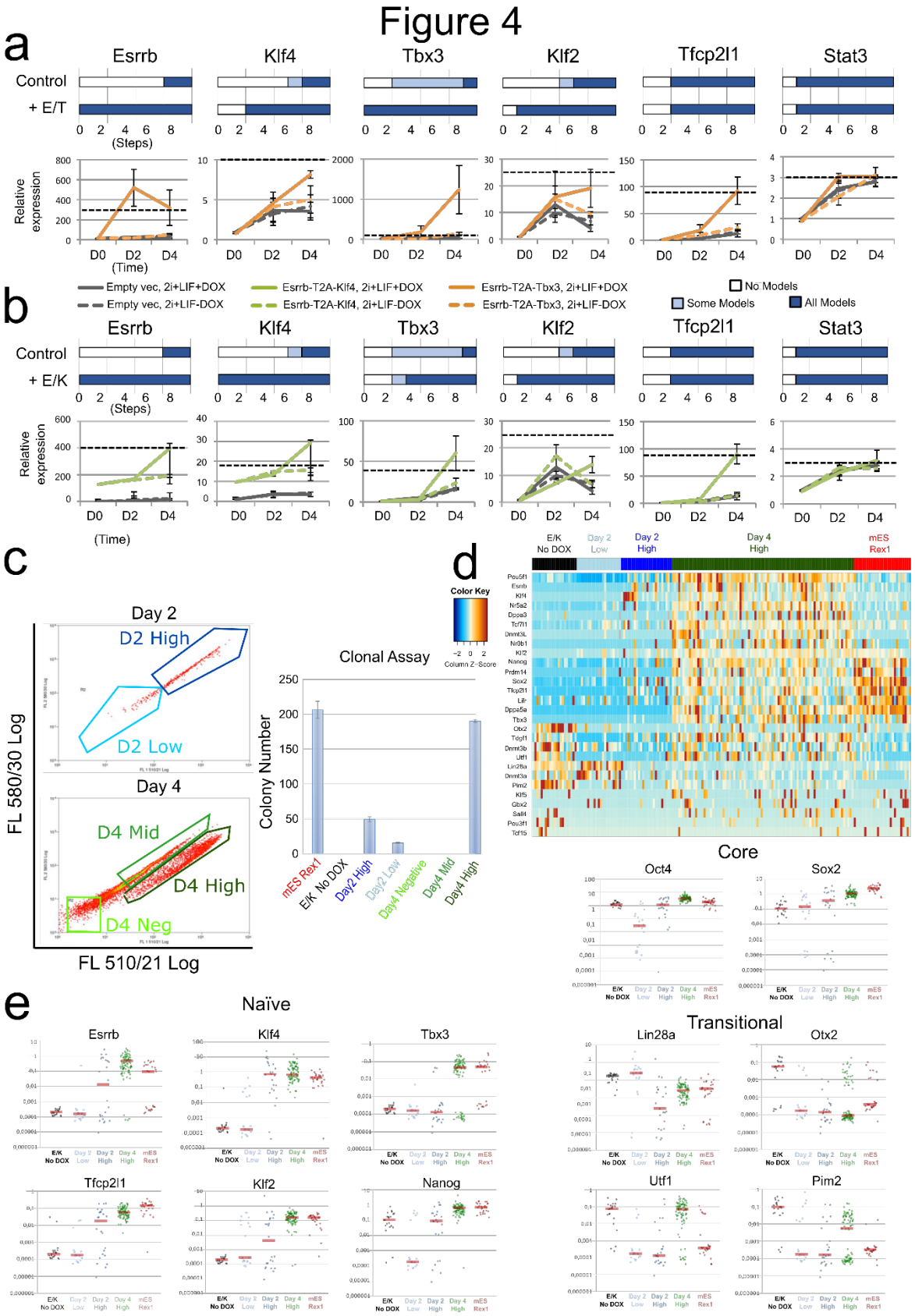

Figure 4: Co-expression of late-activated factors increases pluripotency marker expression and significantly reduces the resetting time scale. See also Fig. S3, S5, Table S1. (a) Top: Predictions of

the number of regulation steps required for full activation of the indicated gene under control or dual expression of Esrrb and Tbx3 (+E/T). Bottom: Gene expression of EpiSCs harbouring empty vector (grey) or Esrrb/Tbx3 (orange), captured at D0 (F/A), D2 and D4 (as described in Fig. 3d). Dashed black line: expression levels in ESCs maintained in 2i+LIF. Data normalised to empty vector cultures in F/A. Gapdh serves as an internal control. Mean +/- SEM, n=3. (b) As for (a), comparison of control with dual expression of Esrrb and Klf4 (+E/K, green in bottom plot). (c) Left: Flow cytometry profiles of resetting progression of EpiSCs stably transfected with the Esrrb-T2A-Klf4 construct and cultured in 2i+LIF with DOX for 2 and 4 days, with indicated fractions of cells sorted for colony formation assay. Since the Venus reporter is under the control of a DOX responsive element, and the emission spectra of Venus and GFP fluorescence overlap, Oct4-GFP reporter expression could not be fully distinguished from Venus fluorescence. Right: number of AP^+ colonies formed from 250 sorted cells from indicated fractions. (d) Heatmap of single-cell expression of major ESC and EpiSC markers in un-induced EpiSCs (black), established ESCs (Red) and Day 2 High/Low (dark and light blue) and Day 4 High cells (green). (e) Scatterplots of single-cell expression of pluripotency and transitional markers. Red bar, median gene expression.

Figure 5

a

Prediction	EpiSC	Day 2 Low	Day 2 High	Day4	ES
Klf2 Tbx3	1.000	0.571	0.500	0.000	0.037
Klf2 Tbx3	0.000	0.381	0.375	0.233	0.333
Klf2 Tbx3	0.000	0.048	0.125	0.744	0.593
X Klf2 Tbx3	0.000	0.000	0.000	0.023	0.037

Proportion of cells

0 1

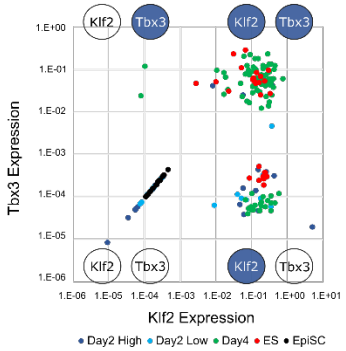

Prediction	EpiSC	Day 2 Low	Day 2 High	Day4	ES
Klf2 Gbx2	1.000	0.429	0.458	0.023	0.037
Klf2 Gbx2	0.000	0.381	0.417	0.802	0.741
Klf2 Gbx2	0.000	0.048	0.083	0.174	0.185
X Klf2 Gbx2	0.000	0.143	0.042	0.000	0.037

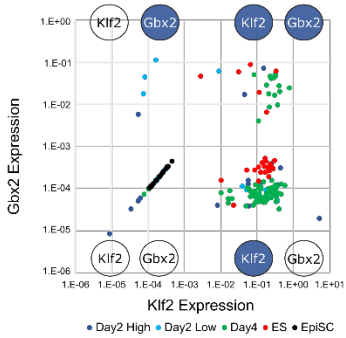

Prediction	EpiSC	Day 2 Low	Day 2 High	Day4	ES
Sox2 Tfcp2l1	0.000	0.190	0.208	0.000	0.000
Sox2 Tfcp2l1	0.905	0.667	0.167	0.000	0.037
Sox2 Tfcp2l1	0.095	0.095	0.583	1.000	0.963
X Sox2 Tfcp2l1	0.000	0.048	0.042	0.000	0.000

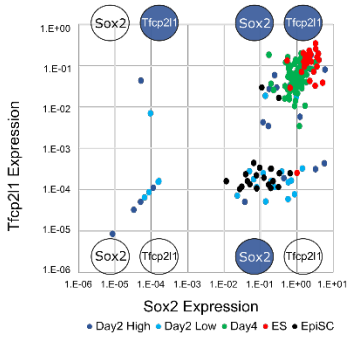

b

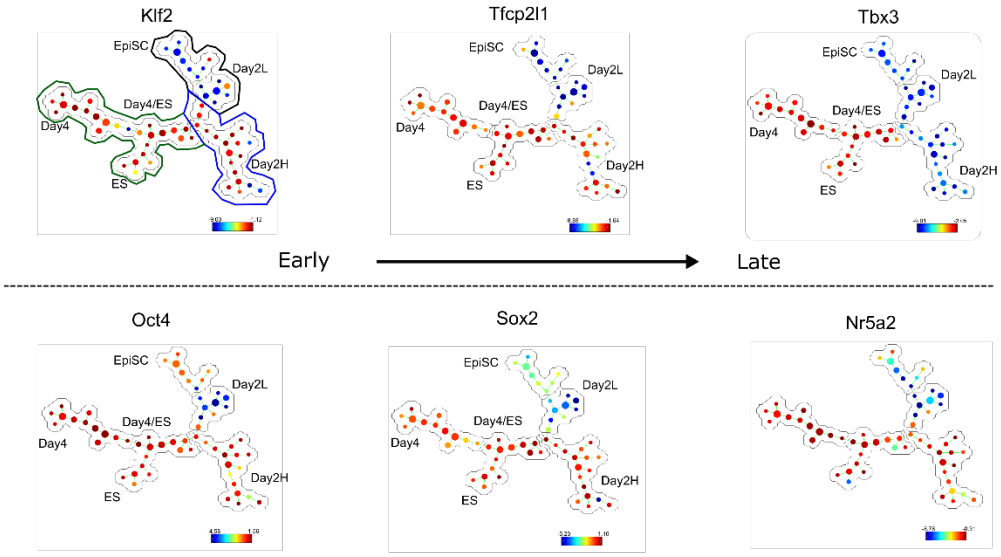

Figure 5: Single cell gene expression profiles recapitulate predicted sequence of gene activation. (a) Left panel: predictions from the 0.782 cABN of the sequence of gene activation between gene pairs (white, off; blue, on) along the resetting trajectory compared to single cell gene expression measured by RT-qPCR. Table summary of the percentage of single cells at the indicated stage of resetting

(column) that have the indicated expression state. Right Panel: Scatterplots showing single cell coordinates based on the expression of the gene pair. (b) SPADE analysis of single cell gene expression of naïve network components along the resetting trajectory, where clusters are coloured according to the expression of the indicated factor. Outlined on the Klf2 plot are the groups of cells that have lost resetting capacity (black), the potential intermediates (blue) and those that have reached the naïve state (green).

Figure 6

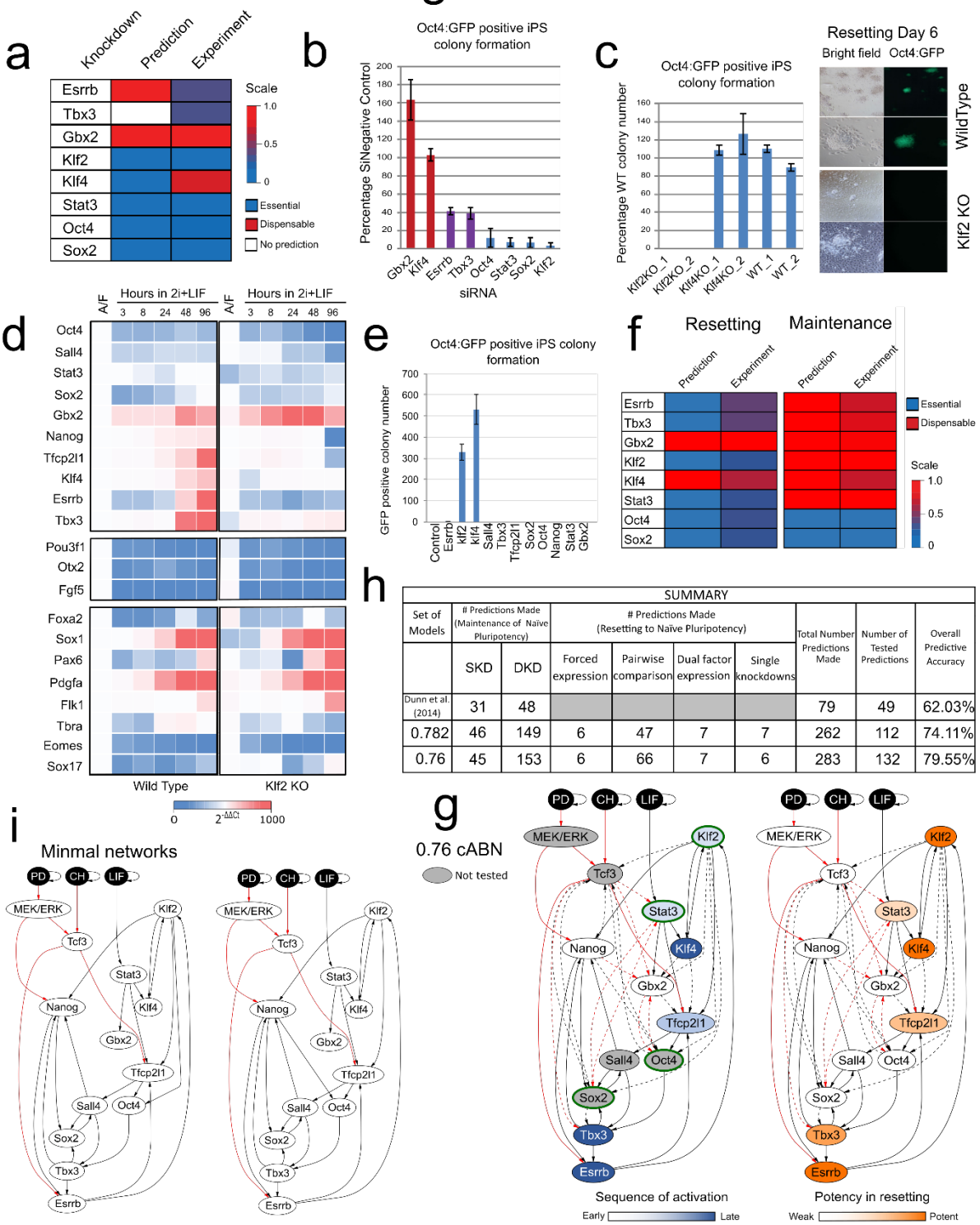

Figure 6: Klf2 is a potent and required factor for naïve network resetting, but not for maintenance of pluripotency, whereas Klf4 is dispensable. See also Fig. S6, Tables S2-4. (a) Predictions from the 0.782 cABN of factors that are essential or dispensable for resetting, compared against experiment results shown in b. (b) siRNA knockdown effect measured by percentage clonogenicity, relative to negative control. (c) Left, resetting of Klf2 and Klf4 KOs EpiSCs measured by Oct4:GFP colony formation capacity. Right, representative images of wild type and Klf2 KO EpiSC resetting at day 6. (d) Gene expression of network components in wild type and Klf2 KO EpiSCs during resetting. (e) Klf2 KO EpiSC

resetting can only be rescued by transient expression of Klf2 and Klf4. (f) A summary of the effect of single factor knockdowns on maintenance and resetting towards naïve pluripotency. Predictions generated from the refined 0.76 cABN. (g) The 0.76 cABN, here used to illustrate the kinetics of EpiSC resetting. Left: Genes coloured according to the order of activation during resetting in 2i+LIF. Right: Genes coloured according to their potency in enhancing the efficiency of resetting. TFs with a green border are indispensable for resetting. (h) A summary table showing the number of predictions and overall predictive accuracy of the cABNs, as they are further refined against experimental observations. (i) The two minimal network topologies from the 0.76 cABN.

Figure 7

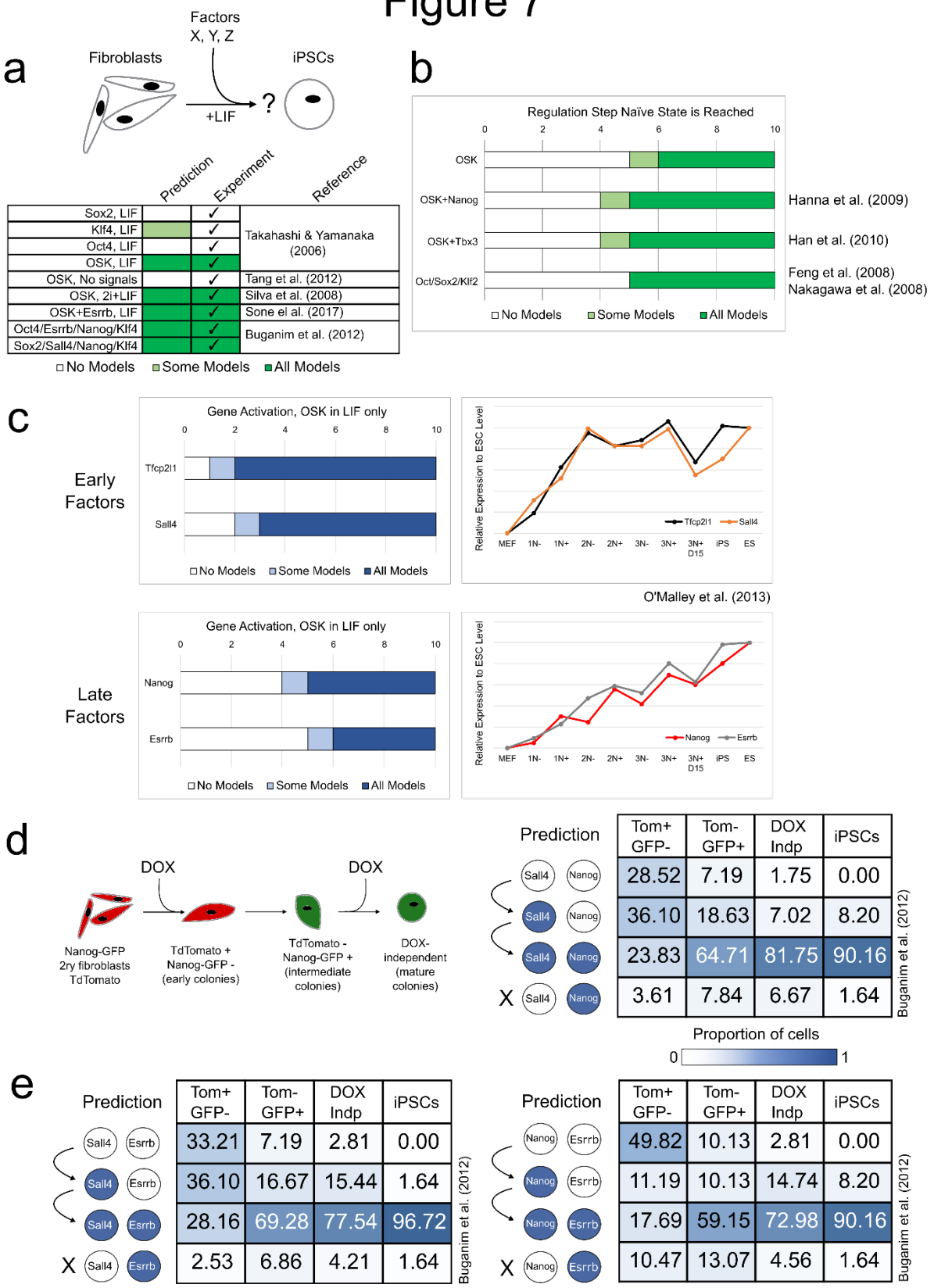

Figure 7: A common gene regulatory program governs naïve state maintenance and reprogramming from somatic cells. (a) Top, somatic cell reprogramming with different factor combinations can be investigated using our models. Bottom, identification of gene combinations that do (dark green) or do not (white) enable reprogramming using the 0.76 cABN, without further training these models using

experimental data from MEF reprogramming. All combinations for which the model analyses generated conclusive outcomes are in agreement with published data, as indicated by the ticks and citations. (b) Identification, by examination of network trajectories, of factor combinations yielding enhanced reprogramming efficiency compared to Oct4/Sox2/Klf4 (OSK), which agree with the published experimental observations indicated. (c) Recapitulation of the activation kinetics of individual genes during somatic cell reprogramming. Left, the number of regulation steps required for permanent activation of the indicated gene; Tfcp2l1 and Sall4 are found to be early-activated factors, while Nanog and Esrrb are late-activated. Right, gene expression of indicated factor extracted from O'Malley et al. (2013) for sorted populations of reprogramming intermediates validates early and late gene activation. (d) Diagram showing the experimental scheme used to generate reprogramming intermediates analysed by single-cell RT-qPCR in Buganim et al. (2012). (e) Predictions of the sequence of gene activation along the reprogramming trajectory in OSK+LIF compared with measured single cell expression patterns from Buganim et al. (2012). Each table shows the percentage of single cells at the indicated stage of reprogramming (column) that have the indicated expression state of the gene pair considered (row).

Supplementary Figure 1

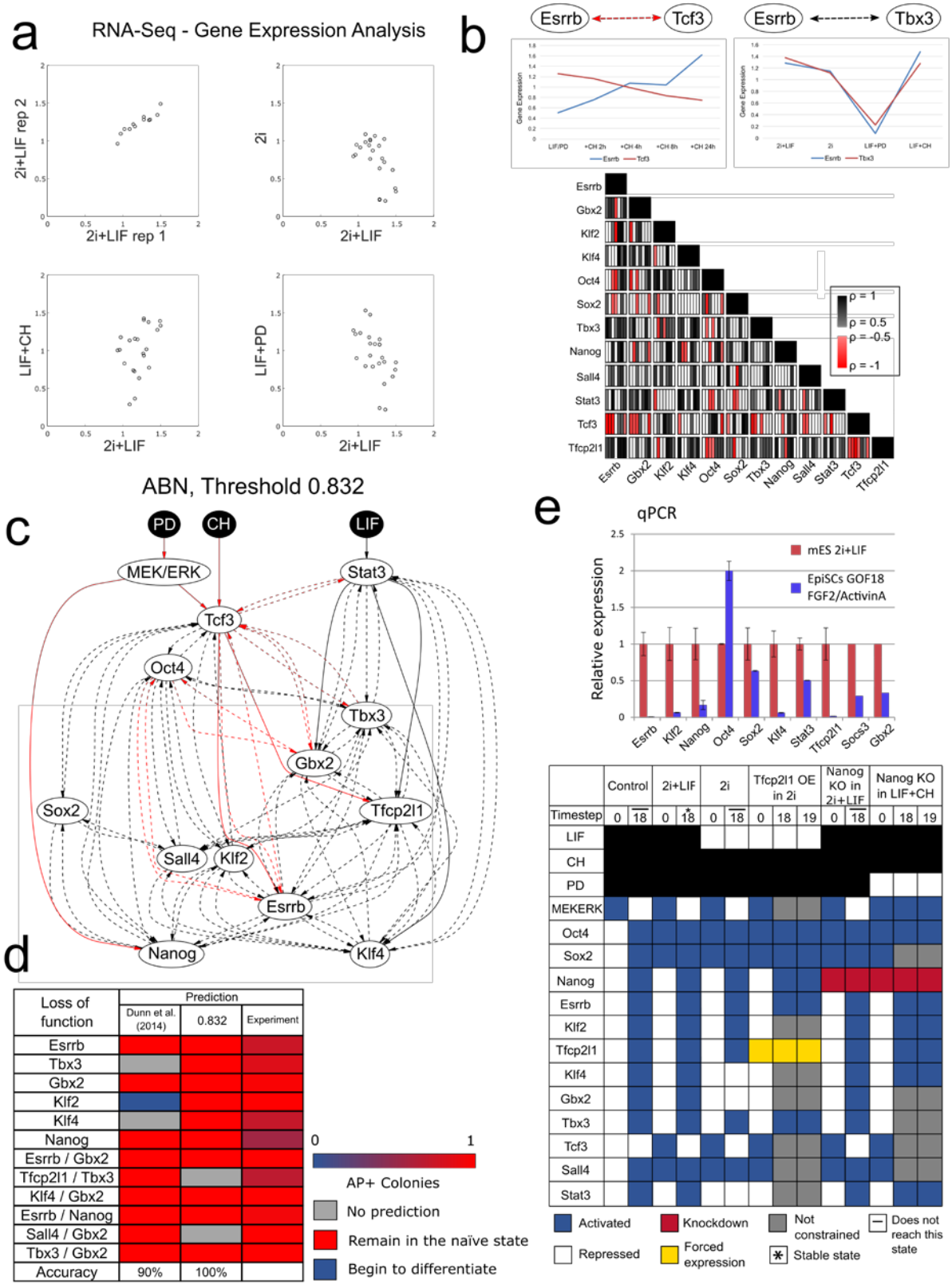

Figure S1, related to Fig. 1: Deriving and constraining the 0.832 ABN. (a) RNA-Seq expression data for 12 naive network components, measured in the four possible combinations of LIF, CH and PD. (b) Top, gene expression correlation between gene pairs is used to infer possible interactions. Strong negative correlation indicates a possible negative interaction; strong positive correlation indicates a possible

positive interaction. Correlation does not inform which gene could be the regulator, so possible interactions are bidirectional. Bottom, Pearson coefficients for each gene pair for six qRT-PCR and one RNA-sequencing expression datasets. Red: negative coefficient below -0.5. Black: positive coefficient above 0.5. (c) The ABN defined by a Pearson correlation threshold of 0.832. This is refined to become the 0.832 cABN (Fig. 1b) once constraints have been imposed, and required and disallowed interactions have been identified. (d) Comparing predictions for the 0.832 cABN against the maintenance cABN derived by Dunn et al. (2014). Here, the predictions correspond to whether an ESC will remain in the self-renewing state under the indicated knockdown. Note an increase in the number of predictions, with incorrect predictions corrected in the refined 0.832 cABN. (e) Top, Relative gene expression of naïve network components in GOF18 EpiSCs compared to ESCs grown in 2i+LIF. Bottom, discretisation of gene expression patterns to define the six resetting experimental constraints depicted in Fig. 1c. Each constraint consists of an initial (timestep 0) and final state (timestep 18), which is either stable (asterisk) or unreachable (bar). Components may be knocked down (red) or under forced expression (yellow). If a specific gene expression is unknown, it is unconstrained (grey).

Supplementary Figure 2

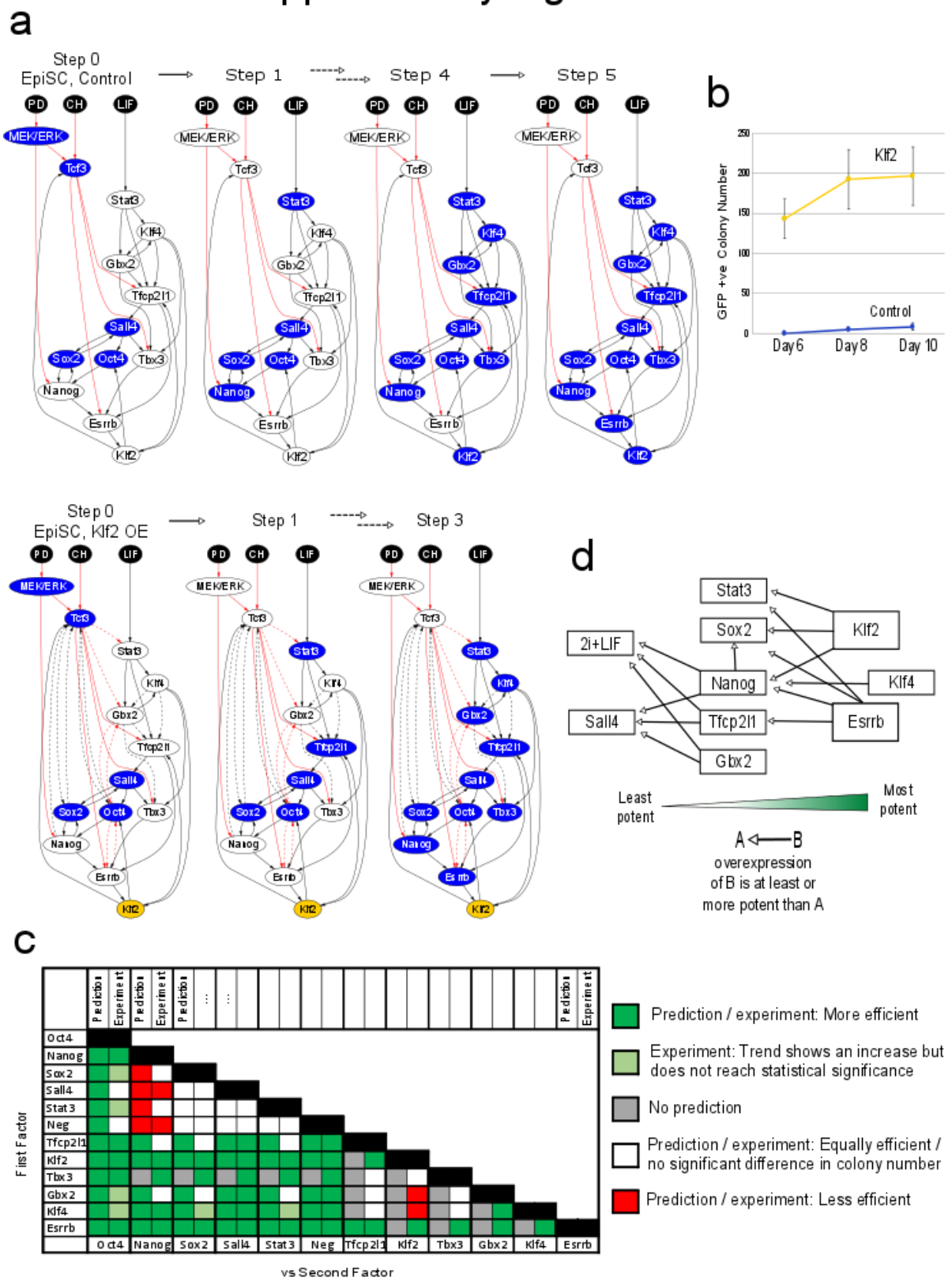

Figure S2, related to Fig. 1: Predicting the relative potency of single factor forced expression in enhancing resetting to the naïve state. (a) Schematic representation of network progression with forced expression of Klf2, which allows the network to stabilise in the naïve state in fewer steps compared to control in 2i+LIF (Fig. 1F). (b) Oct4:GFP^{+} colony number measured over the resetting time

course under empty vector control and forced Klf2 expression. (c) Summary table of the predicted relative resetting efficiency of each pair of components compared with experimental results. Each row compares the prediction from the 0.782 cABN with experiment, showing whether the first factor (row) is more/less potent (green/red) than the second factor (column). We show experimental results where there was a significant difference between the resulting colony number (Student's t-test, $p<0.05$). In none of the cases tested were the predictions in disagreement with the experimental results (i.e. prediction of gene X being more efficient than gene Y, when in fact gene Y was significantly more efficient than X). (d) Schematic summary of results shown in c.

Supplementary Figure 3

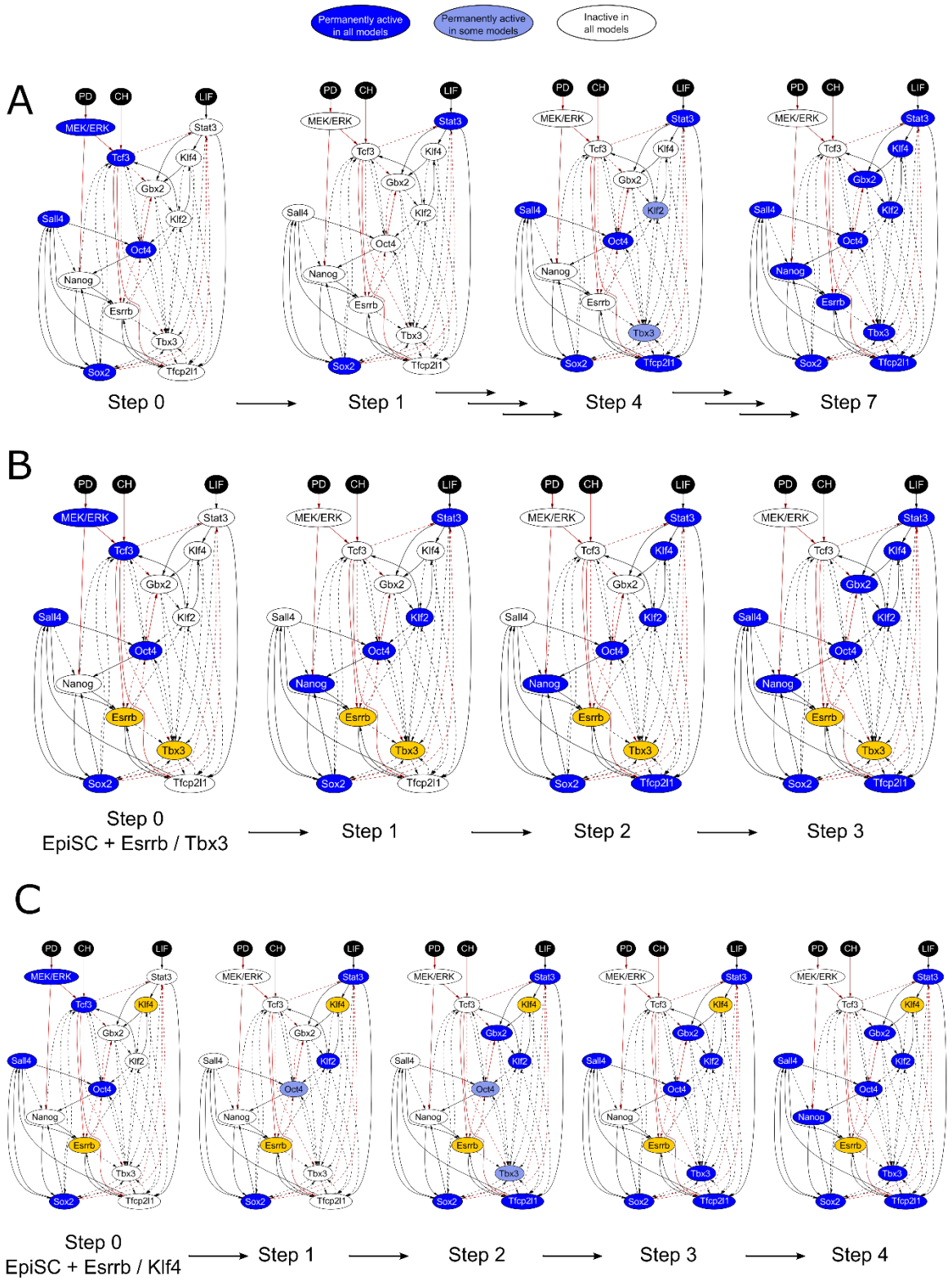

Figure S3, related to Fig. 3 and Fig. 4a, b: A comparison of the resetting kinetics under empty vector control and dual factor expression, visualised on the 0.782 cABN. (a) Resetting under 2i+LIF alone, which takes 7 steps to stabilise in the naïve state. (b) Resetting under dual expression of Esrrb and

Tbx3 in 2i+LIF, which takes 3 steps to stabilise in the naïve state. (c) Resetting under dual expression of Esrrb and Klf4 in 2i+LIF, which takes 4 steps to stabilise in the naïve state.

Supplementary Figure 4

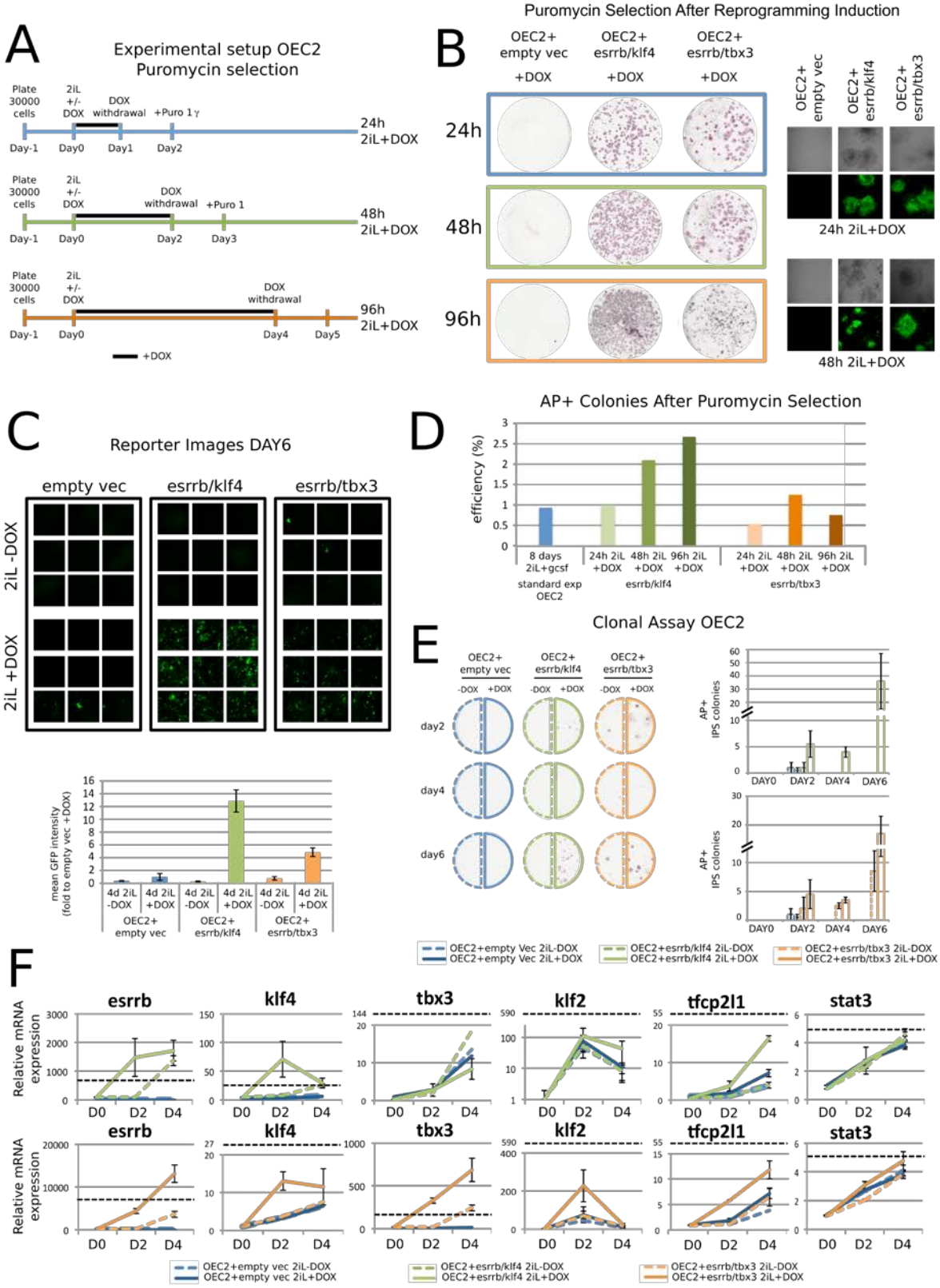

Figure S4, related to Fig. 3: Investigating dual factor expression in OEC2-GY118 EpiSCs. (a) Experimental scheme for the functional characterisation of Esrrb-T2A-Klf4 or Esrrb-T2A-Tbx3 forced expression in OEC2 EpiSC resetting. (b) Left: Representative images of AP staining of reset colonies generated from OEC2 Y118 EpiSCs stably transfected with a piggyBac empty vector or with a piggyBac vector harbouring Esrrb-T2A-Klf4 or Esrrb-T2A-Tbx3. Cells were treated with 2i+LIF to induce resetting and with DOX for 24h, 48h and 96h (grey, green and orange boxes) to induce transgene expression. Puromycin selection was applied 24 hours after DOX withdrawal and AP staining performed at day 8 of resetting. Right: Representative confocal images of Puromycin selected Oct4-GFP$^+$ colonies from 1 or 2 days of DOX treatment. (c) Top: Representative confocal images of OEC2 Y118 EpiSCs expressing Esrrb-T2A-Klf4, Esrrb-T2A-Tbx3 or the empty vector control at day6 of resetting. Bottom: Quantification of Oct4-GFP signal at day6 of resetting. Mean GFP intensity was normalised to empty vector. Mean +/- SEM, n=2. (d) Percentage of AP+ colonies in each condition relative to the control treatment. Control treatment is 2i+LIF with GCSF for 8 days, shown in blue. Cells expressing Esrrb-T2A-Klf4 (green) or Esrrb-T2A-Tbx3 (orange) were treated with 2i+LIF and DOX for 1, 2 or 4 days represented by light, medium and dark green respectively. One representative experiment is shown. (e) Left: Representative images of AP staining of colonies generated from resetting OEC2 Y118 EpiSCs stably transfected with an empty vector (blue) or with a piggyBac vector containing Esrrb-T2A-Klf4 (green) or Esrrb-T2A-Tbx3 (orange). Cells were treated with 2i+LIF with or without DOX for 2/4/6/8 days (dashed versus solid line). Clonal assay (300 cells/well) was initiated 24h after DOX treatment and colonies were stained after 8-10 days of culture in 2i+LIF. Right: Quantification of number of AP$^+$ colonies generated from clonal assay performed at day2/4/6/8 of reprogramming of Esrrb-T2A-Klf4 (top) and Esrrb-T2A-Tbx3 (bottom) expressing cells. Mean +/- SEM, n=2. (f) Relative expression of network components in F/A, at day 2 and 4 of resetting in the presence or absence of DOX. Black dashed line indicates expression levels in mouse ESCs maintained in 2i+LIF. Gapdh served as an internal control. Mean +/- SEM, n=2.

Supplementary Figure 5

A

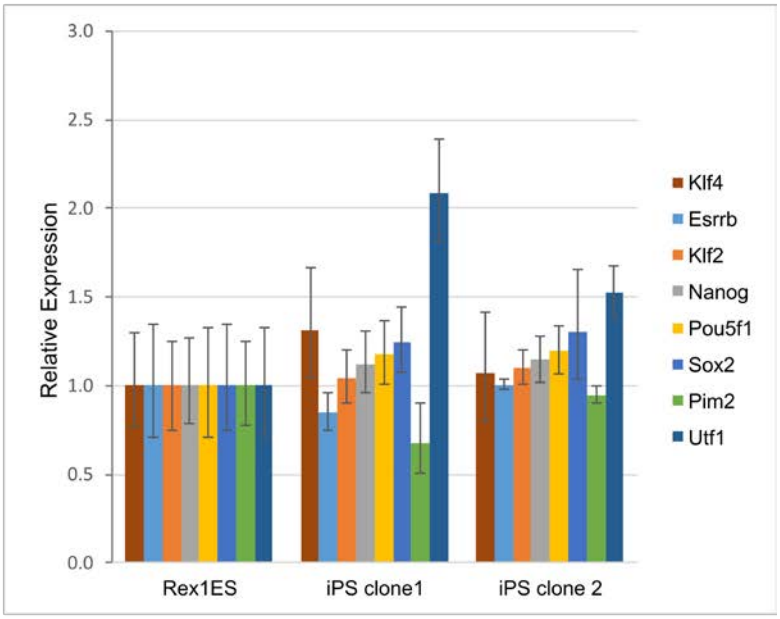

B

Figure S5, related to Fig. 4: Gene expression analysis of two reset clones generated by forced expression of Esrrb-T2A-Klf4 for 4 days (see Fig. 4) and cultured for 3 passages in 2i+LIF without DOX. (a) Expression of naïve and early differentiation markers is comparable to Rex1-GFP mESCs contrasted with Day4 high cells. (b) Contribution to adult chimeras after blastocyst injection of two reset clones confirmed naïve pluripotent identity after resetting by Esrrb/Klf4 dual expression.

Supplementary Figure 6

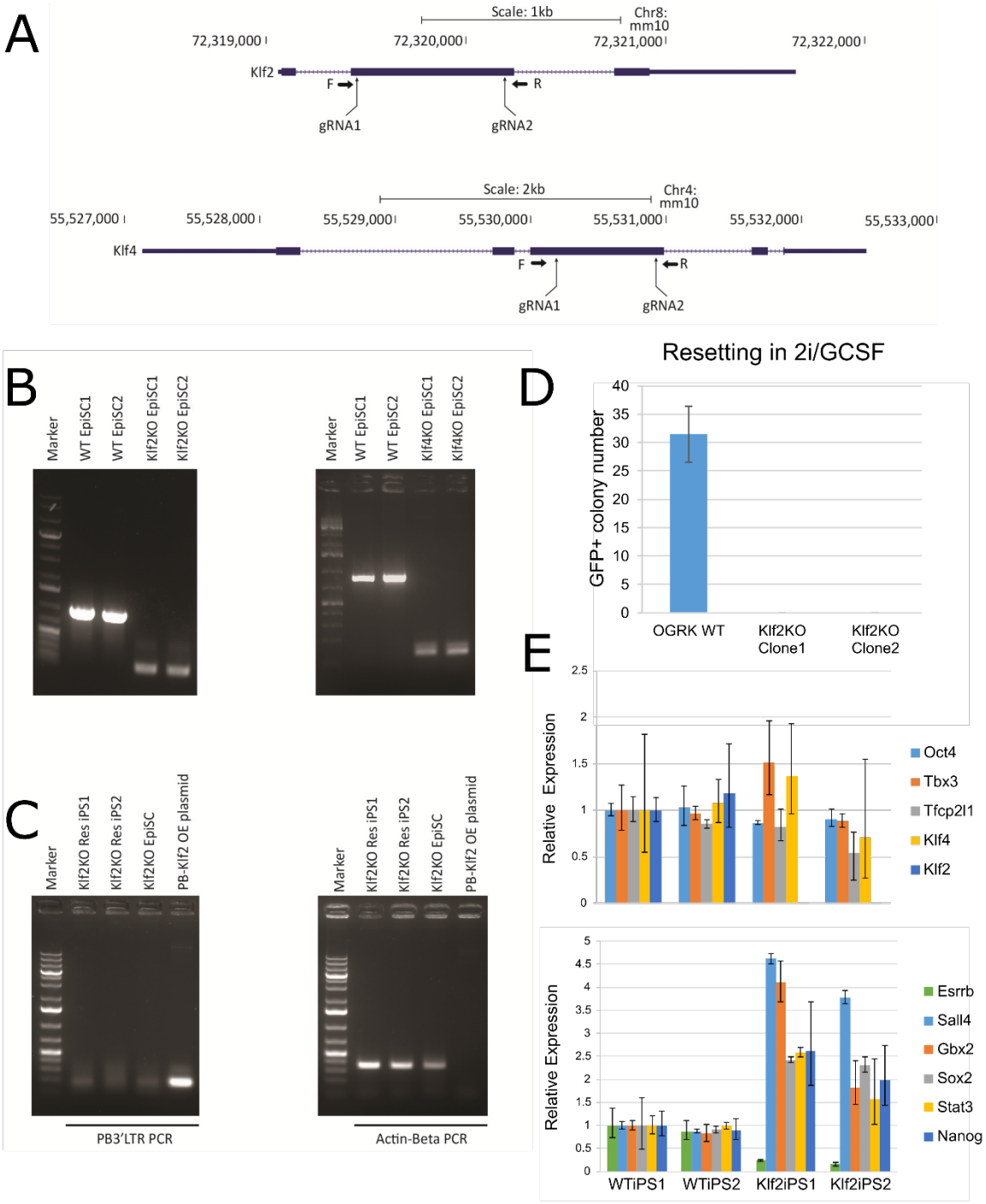

Figure S6, related to Fig. 6: Klf2 and Klf4 KO EpiSC generation and transgene free Klf2KO iPSCs. (a) Strategies for generating Klf2 and Klf4 KO GOF18 EpiSCs using CRISPR/Cas9. Two guide RNAs were designed to flank the largest coding exons for each gene. (b) Genotyping confirmation for homozygous deletion of Klf2 (left) and Klf4 (right) mutants in two independent clones. (c) Klf2KO reset cells generated by transgene overexpression do not contain the transgene stable integration, as demonstrated by the genomic PCR detecting transgene plasmid backbone fragment PB3'LTR (left). ActB genomic PCR (right) serves as a PCR control. (d) We derived a new EpiSC line (OGRK) from E5.5

embryo using N2B27 medium supplemented with ActivinA/Fgf2/Xav939 on Fibronectin, which does not reset spontaneously in 2i+LIF. Stable expression of a chimeric GCSF/LIF GY118F receptor (Yang et al., 2010) allows resetting in the presence of 2i+GCSF. We generated Klf2 KO OGRK lines with the strategy described in panel A and observed that in the absence of Klf2, resetting was abolished, as observed in GOF18 EpiSCs. (e) Gene expression of naïve network components in wild type and rescued Klf2 KO reset clones. The values are normalised to wild type reset clone 1 and Actβ is used as the internal reference. Mean+/-SD, n=2.